NASA TECHNICAL NOTE

THEORETICAL STUDY OF ZERO-FIELD ELECTRON WORK FUNCTION OF METAL IMMERSED IN GAS — DIRECT APPLICATION TO CESIUM THERMIONIC DIODE

by Keung P. Luke and John R. Smith

Lewis Research Center
Cleveland, Ohio

THEORETICAL STUDY OF ZERO-FIELD ELECTRON WORK

FUNCTION OF METAL IMMERSED IN GAS -

DIRECT APPLICATION TO CESIUM

THERMIONIC DIODE

By Keung P. Luke and John R. Smith

Lewis Research Center
Cleveland, Ohio

NATIONAL AERONAUTICS AND SPACE ADMINISTRATION

CONTENTS

THEORETICAL STUDY OF ZERO-FIELD ELECTRON WORK

FUNCTION OF METAL IMMERSED IN GAS -

DIRECT APPLICATION TO CESIUM

THERMIONIC DIODE

by Keung P. Luke and John R. Smith

Lewis Research Center

SUMMARY

It is well known that adsorbed gas on a metal surface can change significantly the electron work function of that metal. This phenomenon is of great importance in the field of gaseous thermionic energy conversion.

In an effort to obtain an analytic relation that can predict quantitatively this phenomenon, the variation in the zero-field electron work function of a metal immersed in a gas is studied. This study begins with a general consideration of the dipole moment, the effective polarizability, the mutual interaction energy, and the desorption rate of a system of gas particles adsorbed on a metal surface. With the aid of several simplifying assumptions, two equations are then derived that relate the change in the zero-field electron work function of the metal to its surface temperature and the gas pressure and temperature. As an example, the change in the zero-field electron work function of tungsten immersed in a cesium vapor $\Delta\varphi_e$ is computed and plotted against the ratio of the tungsten surface temperature to the cesium reservoir temperature at cesium reservoir temperatures T_{Cs} of 300°, 400°, 470°, 473°, 500°, and 600° K. It is found that the computed values of $\Delta\varphi_e$ at $T_{Cs} = 470^{\circ}$, 473°, and 500° K fit very well the experimental data of Houston and of Breitwieser on the cesium-tungsten system at the corresponding cesium reservoir temperatures.

INTRODUCTION

It is now generally agreed that in the near future cesium thermionic converters will play a significant role in the conversion of solar and nuclear energy into electrical energy for space application. It is important, therefore, to understand the basic physics of this type of converter. In particular, the dependence of the zero-field electron work function of the emitter on the emitter temperature and cesium reservoir temperature in a cesium thermionic

diode is of great importance and interest.

In this report the variation in the zero-field electron work function of a metal immersed in a gas is studied. This study is divided into three main sections. The first section, CHANGE IN WORK FUNCTION AGAINST COVERAGE, and the related appendixes D, E, and F present a general consideration of the dipole moment, effective polarizability, and interaction energy of a system of gas particles adsorbed on a metal surface. A general equation is derived for the dipole moment of the ith adsorbed particle as a function of the configuration, dipole moment, and polarizability of the other adsorbed particles. With one important difference this general equation is reduced to a well-known form with the assumptions that the configuration is a Topping square array and that the dipole moments as well as the polarizabilities of the adsorbed particles are identical. It will be seen that this difference is in the definition of the effective polarizability associated with each adsorbed particle.

The section COVERAGE AGAINST SURFACE TEMPERATURE, GAS PRESSURE, AND TEMPERATURE deals with the adsorption and desorption rate of gas particles at and from a metal surface, respectively. A general equation is derived for the total desorption rate of adsorbed particles. Equating this desorption rate to the adsorption rate of impinging gas particles leads to a relation from which the gas coverage can be calculated as a function of physical parameters and the empirical variables: surface temperature of the metal, gas pressure, and temperature.

The section APPLICATION TO CESIUM-TUNGSTEN SYSTEM describes a method for determining from experimental data values of parameters to be used in the previously mentioned sections. These parameters are the magnitude of the effective dipole moment $|\vec{m}_{eff}|$ and the effective polarizability α_{eff} of each adsorbed particle, its desorption energy φ_{a0} at zero coverage, and its equilibrium distance $z_0/2$ from the metal surface. The values of these parameters are determined by this simple method for the cesium-tungsten system. Computed curves for the change in zero-field electron work function $\Delta\varphi_e$ against the ratio of tungsten surface temperature to cesium reservoir temperature T_s/T_{Cs} are then presented and compared with the experimental data of Houston (ref. 1) and Roland Breitwieser (unpublished data obtained at the NASA Lewis Research Center).

In short, the problem considered in the section CHANGE IN WORK FUNCTION AGAINST COVERAGE is illustrated in figures 1(a) and (b). The problem consid-

(a) Effect on electron emission. (b) Mutual interaction among adsorbed gas particles. (c) Amount absorbed.
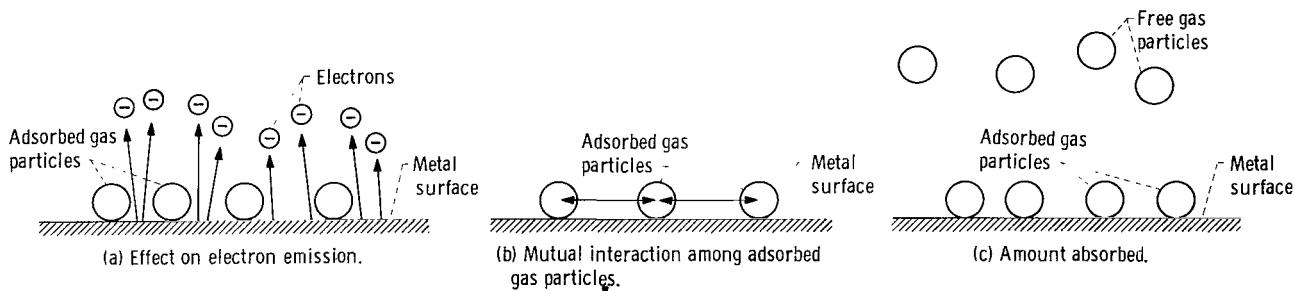
Figure 1. - Adsorption of gas particles on metal surface.

ered in the section COVERAGE AGAINST SURFACE TEMPERATURE, GAS PRESSURE, AND TEMPERATURE is illustrated in figures 1(b) and (c).

Nearly all the working equations used in the text are derived in appendixes B to G, which may be consulted to obtain a more detailed understanding of these equations.

In all the analyses the dipole associated with each adsorbed particle has been treated as an ideal dipole. In addition, it is assumed that the dipole field experienced by each adsorbed particle is uniform and equal to the value at the surface of the metal. The validity of these treatments is examined in appendix H. Finally, in appendix I graphs of the Richardson-Dushman equation are presented.

CHANGE IN WORK FUNCTION AGAINST COVERAGE

When atoms are adsorbed on a metal surface they can be either polarized or ionized and polarized by the metal surface (see appendix D). These polarized adatoms (adsorbed atoms) or polarized adions (adsorbed ions), together with their respective images inside the metal, form an electrical double layer on

(a) Side view; fraction of adsorption sites occupied, $\theta \to 0$.

(b) Top view; fraction of adsorption sites occupied, $\theta > 0$.

(c) Side view; fraction of adsorption sites occupied, $\theta > 0$.
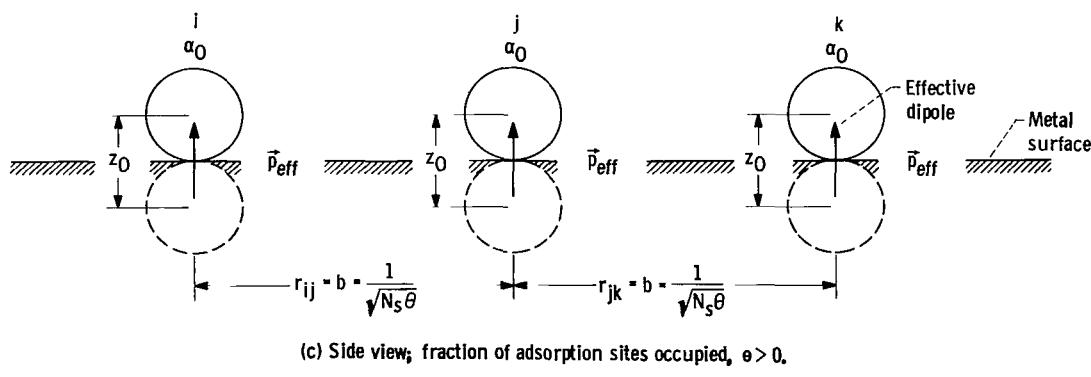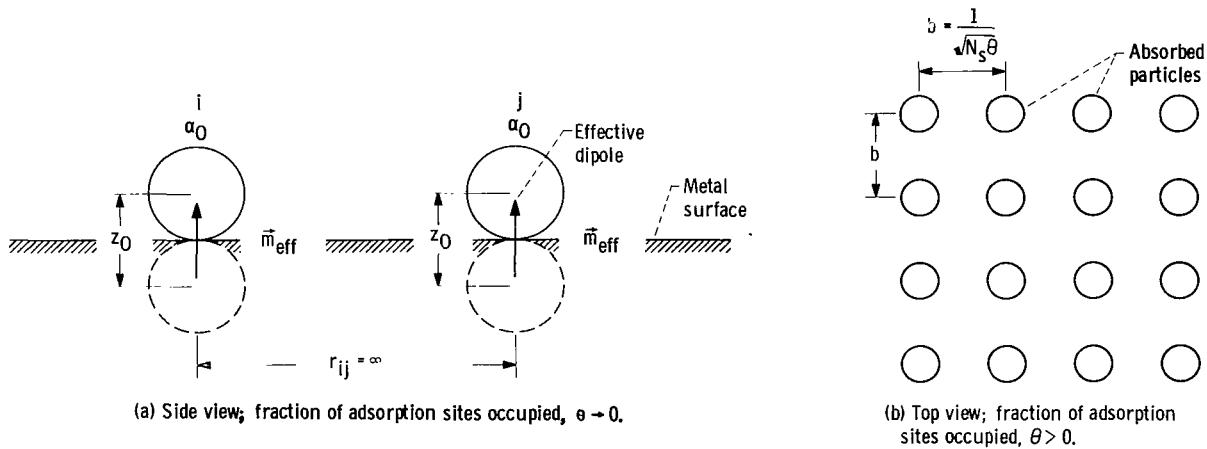
Figure 2. - Topping square array dipole configuration.

the metal surface. Depending on the polarity of this electrical double layer, the electrons leaving the metal surface are either accelerated or retarded by it. Thus, the electron work function of a metal with an adsorbed layer of gas particles on its surface will be changed (refs. 2 to 4). The magnitude of this change is considered in this section.

The model shown in figure 2 is used. All the adsorbed gas particles exist on the surface in an identical state, each possesses the identical scalar polarizability of α_0, and each locates at the same equilibrium distance of $z_0/2$ from the surface. The effective dipole moment $\vec{m}_{eff}$ associated with each adsorbed particle at zero coverage is identical and points in a direction perpendicular to the surface; that is, $\vec{m}_{eff} = \pm|\vec{m}_{eff}|\hat{n}$, where $\hat{n}$ is a unit vector normal to and coming out of the surface. The configuration of these dipoles is that of the planar Topping square array (ref. 5, see figs. 2(b) and (c) also), and there is an infinite number of them on the surface (but the surface density is finite).

The equation (derived in appendix C) for the change in the zero-field electron work function of the metal given by this model is

$$\Delta\varphi_e = -2\pi e N_s (\vec{p}_{eff} \cdot \hat{n})\theta \tag{C5}$$

(Symbols are defined in appendix A.)

An equation for $\vec{p}_{eff}$ (derived in appendix D) is

$$\vec{p}_{eff} = \frac{\vec{m}_{eff}}{1 + 9.033\ \alpha_{eff}(N_s\theta)^{3/2}} \tag{D25}$$

where α_{eff} is given by the relation

$$\alpha_{eff} = \frac{2\alpha_0}{1 - \dfrac{2\alpha_0}{z_0^3}} \tag{D24}$$

Equation (D25) has been used by deBoer (ref. 6), Ehrlich and Hudda (ref. 7), Zingerman, Ishchuk, and Morozovskii (ref. 8), and Gyftopoulous and Levine (ref. 9). None of these scientists, however, have taken into consideration the effect of the metal surface on the value of the effective polarizability to be used in equation (D25). It should be noted that according to equation (D24) this effective polarizability is at least twice the polarizability of the adsorbed particle.

Combining equations (C5) and (D25) yields

$$\Delta\varphi_e = \frac{-2\pi e N_s (\vec{m}_{eff} \cdot \hat{n})\theta}{1 + 9.033\ \alpha_{eff}(N_s\theta)^{3/2}} \tag{1}$$

4

This is the desired equation for the variation in the zero-field electron work function of a metal covered by up to one monolayer (i.e., $\theta = 1$) of adsorbed gas particles.

COVERAGE AGAINST SURFACE TEMPERATURE,

GAS PRESSURE, AND TEMPERATURE

The surface of a metal immersed in a gas is constantly bombarded by the gas particles. At steady state the adsorption rate of impinging gas particles is balanced by the desorption rate of adsorbed particles, thus keeping the fractional coverage of the adsorbed particles on the metal surface θ at a constant value. In this section the kinetic method of equating the adsorption to the desorption rate is used to derive an equation for this fractional coverage as a function of the metal surface temperature, gas pressure, and temperature.

Adsorption Rate

The adsorption rate of impinging gas particles is assumed here to be given by the relation

$$\mu = \frac{\gamma p_g}{(2\pi m_g k T_g)^{1/2}} \tag{2}$$

Desorption Rate

The equation to be derived here for the desorption rate is based on a specific model of the desorption process and desorption energy of the adsorbed particles. This model contains the following features:

(1) There is an infinite number (but finite surface density) of adsorbed particles on the surface.

(2) All adsorbed particles are alike.

(3) An adsorbed particle can desorb as an atom or as an ion.

(4) The ratio of ion to atom desorption rate is given by the Saha-Langmuir equation (ref. 10)

$$\frac{\nu_i}{\nu_a} = \frac{\omega_i}{\omega_a} \exp\left(\frac{\varphi_e - I}{kT_s}\right)$$

(5) The atom desorption rate is given by the equation

$$\nu_a = \frac{N_s \theta f(\theta)}{\tau_0 \exp\left(\dfrac{\varphi_a}{kT_s}\right)}$$

where

$f(\theta)$ term accounting for short-range repulsive forces that act when adsorbed particles come into contact (ref. 11),

$$\frac{1}{1 - \theta} \exp\left(\frac{1}{1 - \theta}\right)$$

$N_s \theta$ surface density of adsorbed particles

$\ln[\theta f(\theta)]$ Langmuir's   S   term given by relation

$$\ln[\theta f(\theta)] = S = \ln\left(\frac{\theta}{1 - \theta}\right) + \frac{1}{1 - \theta}, \text{ eq. (85) of ref. 11}$$

and eq. (8) of ref. 12

$[\tau_0/f(\theta)]\exp\left(\dfrac{\varphi_a}{kT_s}\right)$ average time an adsorbed particle spends on surface before desorbing as an atom

(6) The change $\Delta\varphi_e$ in the electron work function and the change $\Delta\varphi_a$ in the atom desorption energy are for the case in which the model for the adsorbed particles is identical to the one used in the section CHANGE IN WORK FUNCTION AGAINST COVERAGE.

The total desorption rate ν from a unit surface area is given by the relation

$$\nu = \nu_a + \nu_i = \frac{N_s \theta f(\theta)}{\tau_0} \exp\left(\frac{-\varphi_a}{kT_s}\right)\left[1 + \frac{\omega_i}{\omega_a} \exp\left(\frac{\varphi_e - I}{kT_s}\right)\right] \tag{3}$$

according to the previous model. Substituting

$$\left.\begin{aligned} \varphi_e &= \varphi_{e0} + \Delta\varphi_e \\ \varphi_a &= \varphi_{a0} + \Delta\varphi_a \end{aligned}\right\} \tag{4}$$

and equation (G7) for $\Delta\varphi_a$ into equation (3) leads to the result

$$\nu = \frac{N_s \theta f(\theta)}{\tau_0} \exp\left\{-\frac{\varphi_{a0} - \dfrac{1}{4\alpha_{eff}}\left(1 + \dfrac{\alpha_{eff}}{z_0^3}\right)\left[|\vec{m}_{eff}|^2 - \dfrac{1}{(2\pi e N_s)^2}\left(\dfrac{\Delta\varphi_e}{\theta}\right)^2\right]}{kT_s}\right\}\left[1 + \frac{\omega_i}{\omega_a} \exp\left(\frac{\varphi_{e0} - I + \Delta\varphi_e}{kT_s}\right)\right] \tag{5}$$

which is the desired equation for the total desorption rate.

Coverage at Steady-State Condition

At the steady-state condition the adsorption rate of impinging gas particles is balanced by the desorption rate of adsorbed particles. Thus, setting equation (2) equal to equation (5) yields

$$\frac{\gamma p_g}{(2\pi m_g k T_g)^{1/2}} = \frac{N_s \theta f(\theta)}{\tau_0} \exp\left\{-\frac{\varphi_{a0} - \frac{1}{4\alpha_{eff}}\left(1 + \frac{\alpha_{eff}}{z_0^3}\right)\left[|\vec{m}_{eff}|^2 - \frac{1}{(2\pi e N_s)^2}\left(\frac{\Delta\varphi_e}{\theta}\right)^2\right]}{kT_s}\right\}$$

$$\times\left[1 + \frac{\omega_i}{\omega_a}\exp\left(\frac{\varphi_{e0} - I + \Delta\varphi_e}{kT_s}\right)\right] \quad (6a)$$

When the logarithm of both sides of equation (6a) is taken and the equation is rearranged, the following equation relating θ, p_g, T_g, and T_s is obtained:

$$-\varphi_{a0} + \frac{1}{4\alpha_{eff}}\left(1 + \frac{\alpha_{eff}}{z_0^3}\right)\left[|\vec{m}_{eff}|^2 - \frac{1}{(2\pi e N_s)^2}\left(\frac{\Delta\varphi_e}{\theta}\right)^2\right]$$

$$- kT_s\left\{\ln p_g + \ln\left[\frac{\gamma\tau_0(1 - \theta)}{N_s\theta(2\pi m_g k T_g)^{1/2}}\right]\right.$$

$$\left. - \frac{1}{(1 - \theta)} - \ln\left[1 + \frac{\omega_i}{\omega_a}\exp\left(\frac{\varphi_{e0} - I + \Delta\varphi_e}{kT_s}\right)\right]\right\} \quad (6b)$$

APPLICATION TO CESIUM-TUNGSTEN SYSTEM

In this section equations (1) and (6b) will be used to compute the variation in the zero-field electron work function of tungsten immersed in cesium

7

vapor as a function of the tungsten surface temperature and the cesium reservoir temperature. For this application p_g, T_g, and m_g in equation (6b) are replaced by p_{Cs}, T_{Cs}, and m_{Cs}, respectively, and $\vec{m}_{eff} \cdot \hat{n}$ in equation (1) is replaced by $+|\vec{m}_{eff}|$, since it is known experimentally (see, e.g., ref. 12) that adsorbed cesium lowers the electron work function of tungsten. Thus, for a cesium-tungsten system, equations (1) and (6b) become

$$\Delta\varphi_e = -\frac{2\pi e N_s |\vec{m}_{eff}| \theta}{1 + 9.033 \, \alpha_{eff}(N_s\theta)^{3/2}} \qquad (7)$$

$$-\varphi_{a0} + \frac{1}{4\alpha_{eff}}\left(1 + \frac{\alpha_{eff}}{z_0^3}\right)\left[|\vec{m}_{eff}|^2 - \frac{1}{(2\pi e N_s)^2}\left(\frac{\Delta\varphi_e}{\theta}\right)\right]$$

$$= kT_s\left\{\ln p_{Cs} + \ln\left[\frac{\gamma\tau_0(1-\theta)}{N_s\theta(2\pi m_{Cs}kT_{Cs})^{1/2}}\right] - \frac{1}{1-\theta}\right.$$

$$\left. - \ln\left[1 + \frac{\omega_i}{\omega_a}\exp\left(\frac{\varphi_{e0} - I + \Delta\varphi_e}{kT_s}\right)\right]\right\} \qquad (8)$$

In these two expressions the independent variables are T_{Cs} and T_s, the dependent variables are $\Delta\varphi_e$ and θ, and the parameters are γ, N_s, τ_0, φ_{e0}, I, ω_i/ω_a, α_{eff}, $|\vec{m}_{eff}|$, p_{Cs}, φ_{a0}, and z_0. The next step is to choose or determine an appropriate value for each of these parameters.

<div align="center">

Values for Parameters γ, N_s, τ_0, φ_{e0}, I, and ω_i/ω_a

</div>

The following values are chosen for γ, N_s, τ_0, φ_{e0}, I, and ω_i/ω_a:

$$\left.\begin{array}{c}
\gamma = 1.0 \text{ (ref. 12)} \\[6pt]
N_s = 4.8\times10^{14}/\text{sq cm (ref. 12)} \\[6pt]
\tau_0 = 11\times10^{-13} \text{ sec (ref. 13)} \\[6pt]
\varphi_{e0} = 4.59 \text{ ev} \\[6pt]
I = 3.89 \text{ ev (ref. 14)} \\[6pt]
\omega_i/\omega_a = 1/2 \text{ (ref. 15)}
\end{array}\right\} \qquad (9)$$

8

It should be mentioned that the previous value for τ_0 is determined experimentally for the case of cesium ions desorbing from a polycrystalline tungsten surface. It is, however, a fairly representative value of τ_0 because other experimental data (refs. 15 to 17) and theory (ref. 18) on adsorption time show that τ_0 is generally in the range 10^{-12} to 10^{-14} second.

The value of 4.59 electron volts chosen for the bare electron work function of tungsten φ_{e0} is the average of the values 4.62, 4.56, and 4.60 electron volts. The first value is given by Taylor and Langmuir (ref. 12), while the second and third values are determined from the respective thermionic data of Houston (ref. 1) and Breitwieser.

<div align="center">Values for Parameters α_{eff} and $|\vec{m}_{eff}|$</div>

To obtain values for α_{eff} and $|\vec{m}_{eff}|$, equation (10) is fitted to the data of Taylor and Langmuir (ref. 12) for $-\Delta\varphi_e$ against θ for cesium on tungsten in the range $0 \leq \theta \leq 0.63$. The resultant equation is

$$\Delta\varphi_e = \frac{-8.75\,\theta}{1 + 1.77\,\theta^{3/2}} \qquad (10)$$

which yields
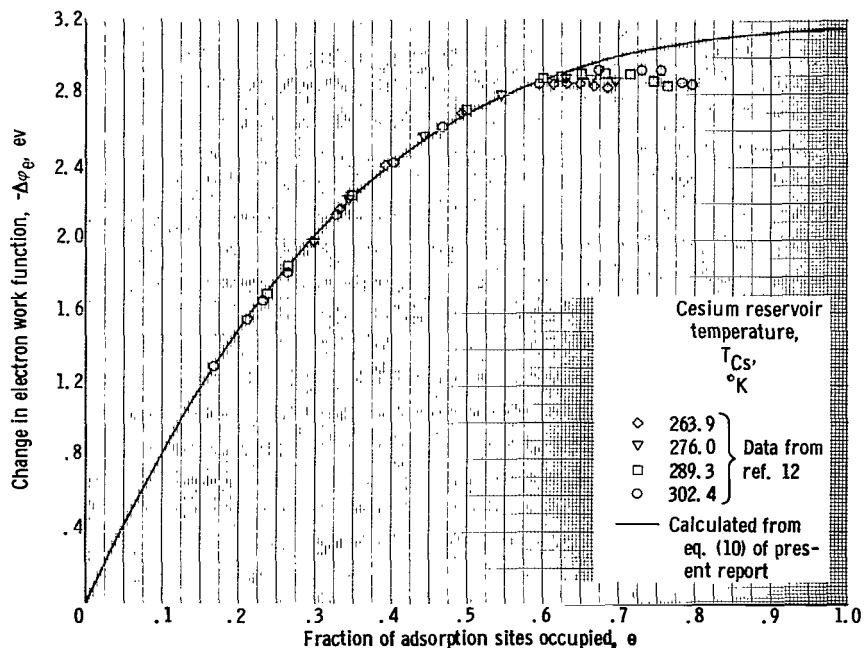
Figure 3. - Comparison of result computed from equation (10) with data of Taylor and Langmuir (ref. 12), cesium-tungsten system.

$$\left.\begin{array}{r} |\vec{m}_{eff}| = 9.70 \text{ Debyes}[1] \\[8pt] \alpha_{eff} = 18.7 \text{ A}^3 \end{array}\right\} \tag{11}$$

Note that $\Delta\varphi_e$ is now expressed solely in terms of θ. Equation (10), together with the data of reference 12, is plotted in figure 3. It is shown there that equation (10) represents the data to within 2 percent up to a coverage of 0.65.

<center>Values for Parameter p_{Cs}</center>

For the values of p_{Cs}, the data of Taylor and Langmuir on the vapor pressure of cesium (ref. 19) will be used. Their data are expressed in the form

$$\ln p_{Cs} = A - \frac{B}{T_{Cs}} \tag{12}$$

where p_{Cs} is in millimeters of mercury and where A and B depend on T_{Cs} as follows:

T_{Cs}, °K	A	B
224 to 302	17.70	9300
302 to 408	16.17	8820
408 to 551	15.76	8660
551 to 745	15.38	8440

<center>Values for Parameters φ_{a0} and z_0</center>

Values for the two remaining parameters φ_{a0} and z_0 are now to be determined. For this purpose, equations (6b) and (12) are combined, and the values given for N_s, τ_0, $|\vec{m}_{eff}|$, and α_{eff} in equations (9) and (11) are substituted into the resultant equation to obtain

---

[1]One Debye equals 10^{-18} (statcoulomb)(centimeter).

$$-\varphi_{a0} + 0.786\left(1 + \frac{18.7}{z_0^3}\right)\left[1 - \left(\frac{\Delta\varphi_e}{8.75\,\theta}\right)^2\right]$$

$$= \frac{T_s}{T_{Cs}}\left[-\frac{B}{11,606} + \frac{T_{Cs}}{11,606}\left(A + \ln\frac{7.02\times10^{-6}(1-\theta)}{T_{Cs}^{1/2}\theta} - \frac{1}{1-\theta}\right.\right.$$

$$\left.\left. - \ln\left\{1 + \frac{1}{2}\exp\left[\frac{11,606}{T_{Cs}(T_s/T_{Cs})}(0.70 + \Delta\varphi_e)\right]\right\}\right)\right] \qquad (13)$$

In this equation φ_{a0} is in electron volts, z_0 is in units of A, and T_s and T_{Cs} are in °K.

The values of φ_{a0} and z_0 are now determined by fitting the computed curve of $-\Delta\varphi_e$ against T_s/T_{Cs} to Houston's data (ref. 1) for cesium on tungsten over the range $0 \leq -\Delta\varphi_e \leq 2.9$ electron volts. This range is chosen because, for $-\Delta\varphi_e > 2.9$ electron volts, the curve of $-\Delta\varphi_e$ against θ computed from equation (10) starts to deviate from the data of Taylor and Langmuir (see fig. 3). Before taking this step, however, it should be mentioned that Houston's data were taken by collecting electrons emitted by a hot surface (emitter) with an accelerating field. Although the field helps the electrons to escape from the emitter, it also turns back the cesium ions desorbed from it. The result is that the total desorption rate ν of the adsorbed cesium particles corresponding to the experimental condition encountered in Houston's experiment is equal to the atom desorption rate ν_a. Therefore, the term

$$\frac{1}{2}\exp\left[\frac{11,606}{T_{Cs}(T_s/T_{Cs})}(0.70 + \Delta\varphi_e)\right]$$

which represents the ratio of cesium ion to cesium atom desorption rate, may be dropped from equation (13). The result is

$$-\varphi_{a0} + 0.786\left(1 + \frac{18.7}{z_0^3}\right)\left[1 - \left(\frac{\Delta\varphi_e}{8.75\,\theta}\right)^2\right]$$

$$= \frac{T_s}{T_{Cs}}\left(-\frac{B}{11,606} + \frac{T_{Cs}}{11,606}\left\{A + \ln\left[\frac{7.02\times10^{-6}(1-\theta)}{T_{Cs}^{1/2}\theta}\right] - \frac{1}{1-\theta}\right\}\right) \qquad (14)$$

Now the step of fitting the computed curve of $-\Delta\varphi_e$ against T_s/T_{Cs} to Houston's data at $T_{Cs} = 473^\circ$ K may be taken. This computed curve is obtained by eliminating θ from equations (10) and (14). The values of φ_{aO} and z_O determined by this method at $T_{Cs} = 473^\circ$ K are

$$\left.\begin{array}{l} \varphi_{aO} = 2.71 \text{ ev} \\[6pt] z_O = 3.00 \text{ A} \end{array}\right\} \tag{15}$$

When these values of φ_{aO} and z_O are substituted into equations (13) and (14), the following equations corresponding to the cases for $\nu_i \neq 0$ and $\nu_i = 0$ are obtained:

For $\nu_i \neq 0$:

$$-1.37 - 1.34\left(\frac{\Delta\varphi_e}{8.75\ \theta}\right)^2 = \frac{T_s}{T_{Cs}}\left[-\frac{B}{11,606} + \frac{T_{Cs}}{11,606}\left(A + \ln\left[\frac{7.02\times10^{-6}(1-\theta)}{T_{Cs}^{1/2}\theta}\right]\right.\right.$$

$$\left.\left.-\frac{1}{1-\theta} - \ln\left\{1 + \frac{1}{2}\exp\left[\frac{11,606}{T_{Cs}(T_s/T_{Cs})}(0.70 + \Delta\varphi_e)\right]\right\}\right)\right] \tag{16}$$

For $\nu_i = 0$:

$$-1.37 - 1.34\left(\frac{\Delta\varphi_e}{8.75\ \theta}\right)^2$$

$$= \frac{T_s}{T_{Cs}}\left(-\frac{B}{11,606} + \frac{T_{Cs}}{11,606}\left\{A + \ln\left[\frac{7.02\times10^{-6}(1-\theta)}{T_{Cs}^{1/2}\theta}\right] - \frac{1}{1-\theta}\right\}\right) \tag{17}$$

Computed Curves of $-\Delta\varphi_e$ Against T_s/T_{Cs} -

Comparison With Data

Equation (17), together with equation (10), is now used to compute points for the curves of $-\Delta\varphi_e$ against T_s/T_{Cs} at various values of T_{Cs}. These curves are represented by the solid lines shown in figure 4.

(a) Cesium reservoir temperature, 473° K. Comparison of result computed from equations (10), (16), and (17) with Houston's data (ref. 1).

(b) Cesium reservoir temperature, 470° K. Comparison of result computed from equations (10) and (17) with Breitwieser's data.

(c) Cesium reservoir temperature, 500° K. Comparison of result computed from equations (10) and (17) with Breitwieser's data.

(d) Cesium reservoir temperatures, 300°, 400°, 500°, and 600° K. Computed from equations (10) and (17).

Figure 4. – Change in electron work function of tungsten emitter immersed in cesium vapor as function of ratio of emitter surface temperature to cesium reservoir temperature.

13

Figure 4(a) compares the computed curves of $-\Delta\varphi_e$ against T_s/T_{Cs} with the data of reference 1 at $T_{Cs} = 473^\circ$ K. In this figure the data are the discrete points. The dotted curve ($\nu_i \neq 0$) is determined from equations (10) and (16), and, as pointed out before, the solid curve ($\nu_i = 0$) is computed from equations (10) and (17). For $-\Delta\varphi_e > 1.05$ electron volts, both computed curves merge together and fit data points quite well. For $-\Delta\varphi_e < 1.05$ electron volts, however, the solid curve follows the data more closely than the dotted curve.

As an additional check on the theory proposed here, especially equations (10) and (17), the computed curves of $-\Delta\varphi_e$ against T_s/T_{Cs} at $T_{Cs} = 470^\circ$ and 500° K are compared with Breitwieser's data[2] at the corresponding cesium reservoir temperatures in figures 4(b) and (c). Again, the fit between the computed curves and the experimental data is quite satisfactory.

To show the effect of increasing the cesium reservoir temperature, the computed curves of $-\Delta\varphi_e$ against T_s/T_{Cs} at $T_{Cs} = 300^\circ$, 400°, 500°, and 600° K are presented in figure 4(d). These curves show that, at constant T_s/T_{Cs}, $-\Delta\varphi_e$ increases with increasing T_{Cs} for T_s/T_{Cs} greater than about 3, but increases with decreasing T_{Cs} for T_s/T_{Cs} smaller than about 3.

Finally, figure 5 is presented to show the range of the saturation current density of a tungsten emitter in a cesium diode as the cesium reservoir temperature is raised from 0° K (vacuum) to 400° K, to 500° K, and finally to 600° K. The points for these saturation current curves are determined from equations (10) and (17), a bare tungsten work func-
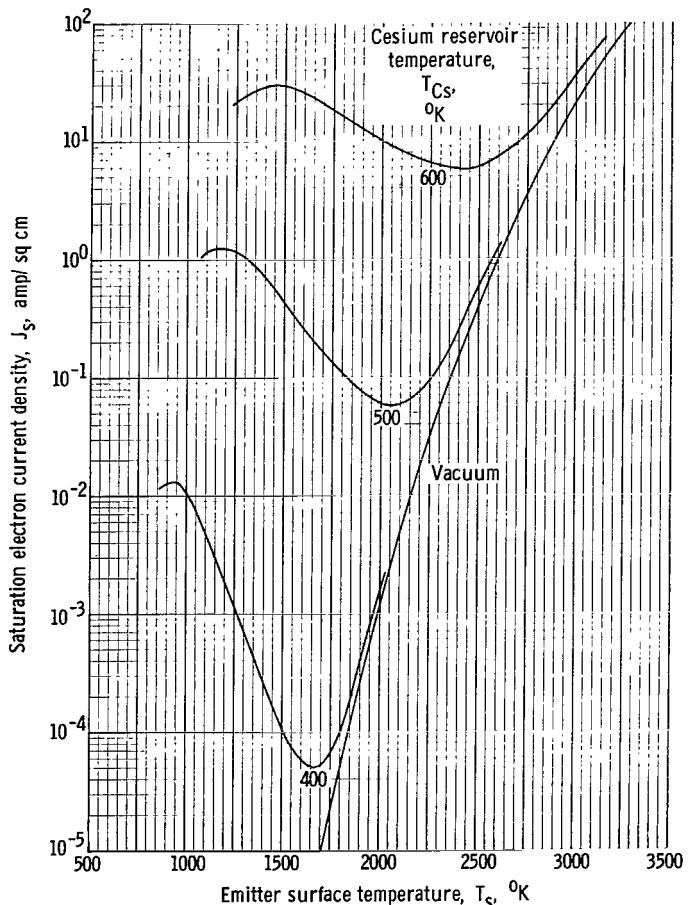
Figure 5. - Computed saturation electron current density of tungsten emitter immersed in cesium vapor as function of emitter surface temperature at cesium reservoir temperatures. Results computed from equations (10), (17), and (11) by using 4.59 electron volts for bare emitter work function.

[2]Breitwieser's data were taken with a planar cesium diode. The emitter structure was formed from tungsten oriented to expose the (110) plane at the emitter surface (ref. 20). The $-\Delta\varphi_e$ of the emitter was determined from its electron saturation current (collected with an accelerating field) and from a bare emitter work function φ_{e0} of 4.60 electron volts.

14

tion of 4.59 electron volts, and graphs of the Richardson-Dushman equation presented in appendix I. The values of J_s at $T_{Cs} = 600^\circ$ K are, in general, several orders of magnitude larger than those at $T_{Cs} = 400^\circ$ K.

Comments on Values of α_0, z_0, φ_{a0}, and $|\vec{m}_{eff}|$

It is worthwhile to comment briefly on the values of α_0, z_0, φ_{a0}, and $|\vec{m}_{eff}|$ determined in this section for the cesium-tungsten system. These values are

$$\alpha_0 = \frac{1}{2} \frac{\alpha_{eff}}{1 + \dfrac{\alpha_{eff}}{z_0^3}}$$

$$= 5.50 \text{ A}^3$$

(see eqs. (D24), (11), and (15)),

$$z_0 = 3.00 \text{ A}$$

$$\varphi_{a0} = 2.71 \text{ ev}$$

(see eq. (15)), and

$$|\vec{m}_{eff}| = 9.70 \text{ Debyes}$$

(see eq. (11)).

In the following table α_0 is compared with the polarizability of a free cesium ion α_{Cs^+} and a free cesium atom α_{Cs^0}:

$\alpha_{Cs^+,exp}$, A^3	2.42 to 3.14	Refs. 21 to 24
$\alpha_{Cs^+,calc}$, A^3	5.60	Ref. 25
$\alpha_{Cs^0,exp}$, A^3	48, 52.5	Refs. 26, 27
$\alpha_{Cs^0,calc}$, A^3	67.7	Ref. 28
α_0, A^3	5.50	Present report

It is seen that α_0 is about equal to $\alpha_{Cs^+,calc}$, but about twice as large as $\alpha_{Cs^+,exp}$. If it is assumed that the experimental value of α_{Cs^+} is a more reliable value of α_{Cs^+} than the calculated value, then it may be concluded that the cesium adsorbed on a tungsten surface is at least partially ionized.

In the following table $z_0/2$ is compared with the radius of a cesium ion R_{Cs^+}, the radius of a cesium atom R_{Cs0}, and Becker's values of $z_0/2$ for a cesium ion adsorbed on the (100) plane $(z_0/2)_{100}$ and on the (110) plane $(z_0/2)_{110}$ of tungsten:

$R_{Cs^+,exp}$, A	1.65 to 1.89	Refs. 29, 30 (p. 92), 31
$R_{Cs0,exp}$, A	2.35, 2.62	Refs. 30 (p. 403), 32
$(z_0/2)_{100}$, A	0.8	Ref. 33 (p. 153)
$(z_0/2)_{110}$, A	1.2	Ref. 33 (p. 153)
$z_0/2$, A	1.50	Present report

This comparison shows that the value of $z_0/2$ determined in this section is not inconsistent with the picture of a partially ionized cesium particle adsorbed on an atomically rough tungsten surface.

The following table presents the value of φ_{a0} determined in this section and those reported in references 12 and 33:

$\varphi_{a0,exp}$, ev	2.79	Ref. 12
$\varphi_{a0,exp}$, ev	2.40	Ref. 33 (p. 152)
φ_{a0}, ev	2.71	Present report

It is interesting to note that the value of φ_{a0} determined in this section falls close to the value of reference 12.

Finally, it is seen that

$$|\vec{m}_{eff}| > Zez_0 \qquad \text{for} \quad Ze < 0.674 \ e$$

This fact is also consistent with the model of an adsorbed cesium particle existing in a polarized, partially ionized ($Ze < 0.674$ e) state on the tungsten surface because (see fig. 10(b))

$$|\vec{m}_{eff}| - Zez_0 = 2|\vec{m}_2| > 0 \qquad \text{for} \quad Ze < 0.674 \ e$$

In summary, it may be stated that the values of α_0, z_0, and $|\vec{m}_{eff}|$ determined in this section are internally consistent and seem to indicate that the adsorbed cesium exists in a polarized, partially ionized state on the tungsten surface.

16

CONCLUDING REMARKS

In this report experimental data have been correlated by means of analytic expressions derived from an explicit model of the adsorbed particle-metal surface interaction. This model gives to the metal surface a hitherto unrecognized role in the adsorption and desorption processes. It is shown herein that the effective polarizability of an adsorbed particle and the variation with coverage of the effective electric field acting on it is increased by the presence of the metal surface.

No consideration is given here to the dependence of various adsorption phenomena investigated herein on the orientation (Miller index) of the metal surface. Also, the possibility that the adsorbed particles may exist on the surface in both the atomic and the ionic state is not considered.

Lewis Research Center
  National Aeronautics and Space Administration
   Cleveland, Ohio, March 23, 1964

APPENDIX A

SYMBOLS

A	constant in cesium vapor pressure equation, eq. (12)
A_O	emission constant in Richardson-Dushman equation, eq. (I1)
$\mathscr{A}$	area of metal surface
a	one-half of distance between positive and negative charges of electric dipole, fig. 6
$\vec{a}$	vector pointing from negative to positive end of dipole
$\vec{a}/a$	unit vector pointing from negative to positive end of dipole
B	constant in cesium vapor pressure equation, eq. (12)
b	distance between nearest neighbors in Topping square array, fig. 2(b)
E	electric field
$\vec{E}_{eff}$	effective electric field acting on adsorbed particle
$\underline{E}_{eff}$	column matrix with elements of $\vec{E}_{eff,1}$, $\vec{E}_{eff,2}$, $\cdots$, $\vec{E}_{eff,\infty}$, eq. (D21)
$\vec{E}_{ik}$	electric field intensity at $\vec{r}_i$ produced by dipole located at $\vec{r}_k$
$\vec{E}_{ik,id}$	electric field intensity at $\vec{r}_i$ produced by ideal dipole located at $\vec{r}_k$
$\vec{E}_{ik,nid}$	electric field intensity at $\vec{r}_i$ produced by nonideal dipole located at $\vec{r}_k$
E_{in}	electric field inside continuous dipole layer
$\vec{E}_{in}$	electric field in region between two sheets of charges of opposite sign
$\vec{E}_P$	electric field produced by dipole at point P
$\vec{E}_{P,id}$	electric field produced by ideal dipole at point P, eq. (B3)
$\vec{E}_{P,nid}$	electric field produced by nonideal dipole at point P, eq. (B5)
e	electronic charge, 4.8×10^{-10}, esu
$f(\theta)$	part of Langmuir's S term, $\dfrac{1}{1-\theta} \exp\left(\dfrac{1}{1-\theta}\right)$

I	ionization potential
$\vec{i}_r$	radial unit vector in polar coordinate
$\vec{i}_\beta$	tangential unit vector in polar coordinate
J_s	saturation current density
k	Boltzmann's constant, $\dfrac{1}{11,606}$ ev/$^\circ$K
k'	defined by eq. (C6)
m	magnitude of $\vec{m}$
$\vec{m}$	dipole moment
m_{Cs}	mass of cesium atom
$\vec{m}_{eff}$	effective dipole moment associated with adsorbed particle at zero coverage, fig. 2(a)
$\underline{m}_{eff}$	column matrix with elements of $\vec{m}_{eff,1}$, $\vec{m}_{eff,2}$, $\cdot\ \cdot\ \cdot$, $\vec{m}_{eff,\infty}$, eq. (D11)
m_g	mass of gas particle
$\vec{m}_1$	dipole associated with adion and its image, fig. 10(b)
$\vec{m}_2$	dipole associated with an adatom, fig. 10(a)
N_s	number of adsorption sites per unit area on metal surface
n	number of particles
$\hat{n}$	unit vector normal to and coming out of surface
p_{Cs}	cesium vapor pressure, eq. (12)
$\vec{p}_{eff}$	effective dipole associated with adsorbed particle at coverage $\theta > 0$, fig. 2(c)
$\underline{p}_{eff}$	column matrix with elements of $p_{eff,1}$, $p_{eff,2}$, $\cdot\ \cdot\ \cdot$, $p_{eff,\infty}$, eq. (D10)
$\langle\vec{p}_{eff}\rangle$	statistical average of $\vec{p}_{eff}$, defined by eq. (E2)
p_g	gas pressure
R_{Cs0}	radius of cesium atom
R_{Cs+}	radius of cesium ion

r	magnitude of $\vec{r}$
$\vec{r}$	positional vector
$\vec{r}/r$	unit vector pointing from center of dipole to point P, fig. 6
r_0	radius of circle with center at origin
r_-	distance from negative end of dipole to point P, fig. 6
r_+	distance from positive end of dipole to point P, fig. 6
$\underline{S}$	diagonal matrix with elements of $2/(z_0)_1^3$, $2/(z_0)_2^3$, $\cdots$, $2/(z_0)_\infty^3$, eq. (D20)
T	temperature, $^{\circ}$K
$\underline{T}$	square matrix, eq. (D9)
T_{Cs}	cesium reservoir temperature, $^{\circ}$K
T_g	gas temperature, $^{\circ}$K
T_s	surface temperature, $^{\circ}$K
t	transposed matrix
$\underline{U}$	unitary matrix
V	total potential energy of adsorbed particles, eq. (F1)
V_{el}	total mutual electrostatic energy of adsorbed particles, eq. (F2)
V_{ex}	total external energy of adsorbed particles, eq. (F4)
V_{in}	total internal energy of adsorbed particles, eq. (F3)
v	mutual electrostatic energy between two adsorbed particles, eq. (E6)
W	total interaction energy between adsorbed particles and metal surface, eq. (F1)
w	interaction energy between single adsorbed particle and metal surface, eq. (E6)
x	x-coordinate
y	y-coordinate
Ze	charge on adion, fig. 10(b)

Z_1	classical configuration integral for one particle, eq. (E7)
Z_∞	classical configuration integral for infinite number of adsorbed particles, eq. (E3)
z	distance above metal surface, fig. 8
z_0	one-half of equilibrium distance of adsorbed particle from metal surface, figs. 2(a), 2(c), 10(b), and 11
α	polarizability
$\underline{\alpha}$	diagonal matrix with elements $\alpha_1, \alpha_2, \cdot\cdot\cdot, \alpha_\infty$, eq. (D19)
α_{Cs^0}	polarizability of cesium atom
α_{Cs^+}	polarizability of cesium ion
α_{eff}	effective polarizability associated with adsorbed particle
$\underline{\alpha}_{eff}$	diagonal matrix with elements $\alpha_{eff,1}, \alpha_{eff,2}, \cdot\cdot\cdot, \alpha_{eff,\infty}$, eq. (D8)
α_0	polarizability of adsorbed gas particle
β	angle between positional vector $\vec{r}$ and dipole $\vec{m}$, fig. 6
γ	sticking coefficient, probability that gas particle striking metal surface will be adsorbed, eq. (2)
ζ	polar angle of positional vector $\vec{r}_k$
η_{ik}	angle between $\vec{p}_{eff,i}$ and vector pointing from center of $\vec{p}_{eff,i}$ to center of kth adsorbed particle
$\underline{\Lambda}$	matrix defined by eq. (D22)
θ	fraction of adsorption sites occupied
μ	arrival rate, eq. (2)
ν	total desorption rate, eq. (5)
ν_a	atom desorption rate
ν_i	ion desorption rate
$\rho^{(n)}(\vec{r}_1, \cdot\cdot\cdot, \vec{r}_n)$	distribution function for n particles, eq. (E5)
$\rho^{(2)}(\vec{r}_1, \vec{r}_2)$	pair distribution function, eq. (E6)
$\rho^{(3)}(\vec{r}_1, \vec{r}_2, \vec{r}_3)$	distribution function for three particles, eq. (E8)

τ	mean adsorption lifetime
τ_0	constant in equation for adsorption lifetime
Φ_P	potential produced by dipole at point P
$\Delta\varphi$	change in desorption energy
φ_a	atom desorption energy at coverage $\theta > 0$
$\Delta\varphi_a$	change in atom desorption energy, eq. (G7)
φ_{a0}	atom desorption energy at zero coverage
φ_e	electron work function at coverage $\theta > 0$
$\Delta\varphi_e$	change in electron work function, eq. (1)
φ_{e0}	electron work function at zero coverage
$\varphi_{i,E_{eff}}$	potential energy of adion in effective field $\vec{E}_{eff}$, eq. (G3)
φ_0	desorption energy at zero coverage
ω_a	statistical weighting factor for atom
ω_{ion}	statistical weighting factor for ion

Subscripts:

exp	experimental
calc	calculated
id	ideal
i,j,k,l,m	i^{th}, j^{th}, k^{th}, l^{th}, and m^{th} adsorbed particles, $0,1,2,\cdots,\infty$
nid	nonideal
x	adsorbed particle, $x = i, j, k, l, \cdots$

GENERAL EQUATION FOR ELECTRIC FIELD OF ELECTRIC DIPOLE (IDEAL

AND NONIDEAL) AS FUNCTION OF DISTANCE FROM DIPOLE

In this report the physical model used for each adsorbed particle is the electric dipole. In calculating the electric field produced by these dipoles, it is not clear whether they should be considered as ideal or nonideal dipoles. (These two terms will be defined later.) In order to see the difference in the electric field produced by an ideal and a nonideal dipole and how this difference arises, an equation for the electric field of an ideal and a nonideal dipole is derived and compared in this appendix.

Consider the dipole shown in figure 6. The following equation is given for the potential Φ_P:

$$\Phi_P = \frac{Ze}{r_+} - \frac{Ze}{r_-} \qquad (B1)$$
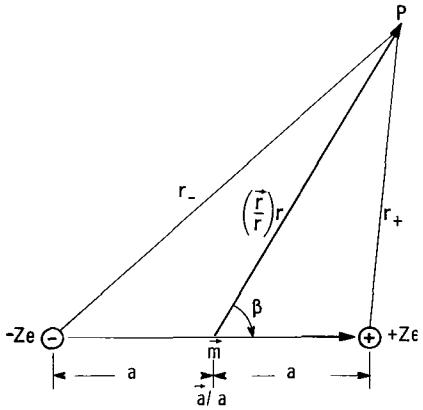
Figure 6. - Dipole geometry.

If the dipole $\vec{m}$ is an ideal dipole (i.e., $2\vec{a}$ approaches zero and Ze approaches infinity in such a way that the product $2Ze\vec{a}$ remains constant and equal to $\vec{m}$), then it may be shown that

$$\Phi_P = \frac{\vec{m} \cdot \vec{r}}{r^3} \qquad (B2)$$

The electric field $\vec{E}_P$ corresponding to this potential is

$$\vec{E}_{P,id} = -\vec{\nabla}\Phi_P$$

$$= \frac{3\vec{m} \cdot \vec{r}}{r^5}\vec{r} - \frac{\vec{m}}{r^3} \qquad (B3)$$

This is the desired equation for the field produced by an ideal dipole. In addition, it should be noted that it is also the correct equation for the field produced by a nonideal (2a > 0) dipole in the region in which the condition r/2a >> 1 holds. As the value of r/2a approaches 1, however, the equation to be derived next for the field should be used.

Equation (B1) is again considered. In terms of the polar coordinates r and β, it may be written as follows:

$$\Phi_P = \frac{Ze}{(a^2 + r^2 - 2ar \cos \beta)^{1/2}} - \frac{Ze}{(a^2 + r^2 + 2ar \cos \beta)^{1/2}} \qquad (B4)$$

The field corresponding to the potential given by equation (B4) is

$$\vec{E}_{P,nid} = -\nabla\Phi_P = \frac{\vec{i}_r}{r^2}\left[\frac{Ze\left(1 - \frac{a}{r}\cos\beta\right)}{\left(1 + \frac{a^2}{r^2} - \frac{2a}{r}\cos\beta\right)^{3/2}} - \frac{Ze\left(1 + \frac{a}{r}\cos\beta\right)}{\left(1 + \frac{a^2}{r^2} + \frac{2a}{r}\cos\beta\right)^{3/2}}\right]$$

$$+ \vec{i}_\beta \frac{m}{2r^3}\sin\beta\left[\frac{1}{\left(1 + \frac{a^2}{r^2} - \frac{2a}{r}\cos\beta\right)^{3/2}} + \frac{1}{\left(1 + \frac{a^2}{r^2} + \frac{2a}{r}\cos\beta\right)^{3/2}}\right] \quad (B5)$$

Figure 7. – Comparison of electric field strength produced by ideal dipole to field strength produced by nonideal dipole.
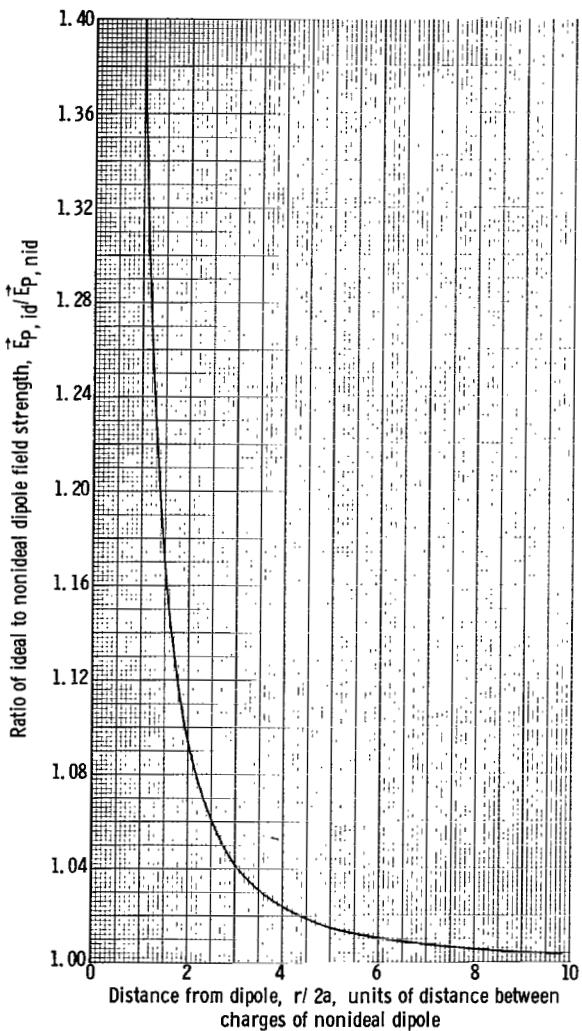
For the important special case where $\beta = 90°$, equation (B5) becomes

$$\vec{E}_{P,nid} = \vec{i}_\beta \frac{m}{r^3}\frac{1}{\left(1 + \frac{a^2}{r^2}\right)^{3/2}} \quad (B6)$$

The deviation of the electric field of an ideal dipole from that of a non-ideal dipole or a real dipole at $\beta = 90°$ is shown in figure 7, which is a plot of the ratio

$$\frac{\vec{E}_{P,id}}{\vec{E}_{P,nid}} = \left(1 + \frac{a^2}{r^2}\right)^{3/2} \quad (B7)$$

against $r/2a$. It is seen that this deviation amounts to +40 percent at $r/2a = 1$ and +1 percent at $r/2a = 6$.

APPENDIX C

EFFECT OF DISCRETE LAYER OF ADSORBED GAS PARTICLES ON ZERO-FIELD

ELECTRON WORK FUNCTION OF METALLIC SUBSTRATE

In this appendix the effect of a discrete layer of adsorbed gas particles on the zero-field electron work function of the metallic substrate is examined. The method used and the result obtained herein are taken from the work of Gavrikyuk (ref. 34). The same model is used here as in the section CHANGE IN WORK FUNCTION AGAINST COVERAGE. This model is shown in figure 8.

There is an infinite number (but a finite surface density) of adsorbed particles, and all adsorbed particles exist in the same state on the surface. Each one is represented by an electric dipole, which, together with its own image in the metal, forms an effective dipole with effective moment $\vec{p}_{eff}$ and effective polarizability $\vec{\alpha}_{eff}$, which are the same for all the adsorbed particles. These effective dipoles take on a planar configuration so that the plane passing through the centers of all these dipoles coincides with the metal surface.

Figure 8. – Electric field intensity produced at $(0, 0, z)$ by dipole $\vec{p}_{eff, k}$ located at $(x_k, y_k, 0)$. Metal surface coincides with x, y-plane at $z = 0$.

The metal surface is the x,y-plane, z is the distance above this plane, $\vec{r}_k(x_k, y_k, 0)$ is the location of the kth effective dipole, and $(\vec{E}_{eff})_k$ is the electric field intensity produced at the point $(0,0,z)$ by the kth effective dipole (see fig. 8). An electron leaving the surface at the point $(0,0,0)$ is acted on by the field $\sum_{k=1}^{\infty} \vec{E}_{eff,k}$. The change in work function for this electron is then given by minus the work done on it by this field as it goes from the point $(0,0,0)$ to the point $(0,0,\infty)$; that is,

$$\Delta \varphi_e = e \sum_{k=1}^{\infty} \int_0^{\infty} \vec{E}_{eff,k} \cdot \hat{n} \, dz \qquad (C1)$$

where $\hat{n}$ is an unit vector normal to and coming out of the x,y-plane. Substituting equation (B3) from appendix B for $\vec{E}_{eff,k}$ in the previous expression leads to the result

$$\Delta\varphi_e = e\vec{p}_{eff} \cdot \hat{n} \left[\sum_{k=1}^{\infty} \int_0^z \frac{2z^2 - r_k^2}{\left(z^2 + r_k^2\right)^{5/2}} \, dz \right]_{z\to\infty} \tag{C2}$$

or

$$\Delta\varphi_e = -e\vec{p}_{eff} \cdot \hat{n} \left[\sum_{k=1}^{\infty} \frac{z}{\left(z^2 + r_k^2\right)^{3/2}} \right]_{z\to\infty} \tag{C3}$$

Since there is an infinite number of adsorbed particles, equation (C3) can be evaluated by the following summation-integration method:

$$\Delta\varphi_e = -e\vec{p}_{eff} \cdot \hat{n} \left[\sum_{k=1}^{k'} \frac{z}{\left(z^2 + r_k^2\right)^{3/2}} + 4zN_s\theta \int_0^{\pi/2} \int_{r_0}^{\infty} \frac{r \, dr \, d\zeta}{\left(z^2 + r^2\right)^{3/2}} \right]_{z\to\infty}$$

$$= -e\vec{p}_{eff} \cdot \hat{n} \left[\sum_{k=1}^{k'} \frac{z}{\left(z^2 + r_k^2\right)^{3/2}} + 2\pi N_s\theta \frac{z}{\left(z^2 + r_0^2\right)^{1/2}} \right]_{z\to\infty} \tag{C4}$$

or

$$\Delta\varphi_e = -2\pi e N_s(\vec{p}_{eff} \cdot \hat{n})\theta \tag{C5}$$

where r_0 is the radius of a circle with its center at the origin. It is related to k' by the equation

$$\frac{k'}{\pi r_0^2} = N_s\theta \tag{C6}$$

It should be added here that the usual and simpler derivation of equation (C5) is made by assuming the dipole layer to be continuous as shown in fig-
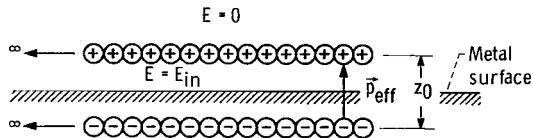
Figure 9. – Continuous dipole layer.

ure 9. In this case, it can be shown by Gauss's law that in the region outside the two sheets of charges the electric field is zero. In the region between the charges the electric field is given by the relation

$$\vec{E}_{in} = -4\pi \frac{\vec{p}_{eff}}{z_0} N_s \theta \qquad (C7)$$

The change in work function for an electron leaving the metal surface is then given by the equation

$$\Delta\varphi_e = e \int_0^{z_0/2} \vec{E}_{in} \cdot \hat{n} \, dz \qquad (C8)$$

Substituting equation (C7) for $\vec{E}_{in}$ in equation (C8) yields

$$\Delta\varphi_e = -2\pi e N_s (\vec{p}_{eff} \cdot \hat{n})\theta \qquad (C9)$$

which is the same as equation (C5).

It is interesting to note that, as long as the dipole layer is infinite in extent, the discrete or the continuous dipole layer assumption leads to an identical expression for the change in the electron work function of the metal.

APPENDIX D

GENERAL EQUATION FOR EFFECTIVE DIPOLE MOMENT ON i^{th}

ADSORBED PARTICLE IN PRESENCE OF INFINITE

NUMBER OF OTHER ADSORBED PARTICLES

An atom adsorbed on a metal surface interacts with that surface. For this reason the electron distribution around its nucleus is distorted. Depending on the magnitude of this distortion, the atom could be classified either as polarized or as ionized and polarized (refs. 2 to 4). This polarized adatom (adsorbed atom) or polarized adion (adsorbed ion), together with its respective image inside the metal, then forms a dipole with effective moment $\vec{m}_{eff}$. For a polarized adatom $\vec{m}_{eff}$ is equal to twice the dipole moment $\vec{m}_2$ of the polarized adatom alone (fig. 10(a)). For a polarized adion, it is equal to the sum
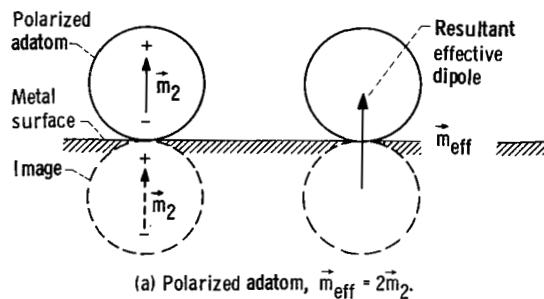
(a) Polarized adatom, $\vec{m}_{eff} = 2\vec{m}_2$.   (b) Polarized adion, $\vec{m}_{eff} = \vec{m}_1 + 2\vec{m}_2$, where $\vec{m}_1 = Zez_0$.
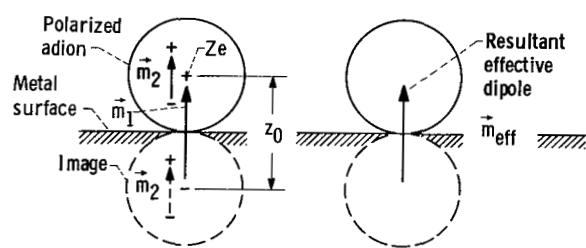
Figure 10. – Polarized adatom and adion and images inside metal.

of the dipole moment $\vec{m}_1$ of the adion and its image plus twice the dipole moment $\vec{m}_2$ of the polarized adion (fig. 10(b)).

Since in the first approximation an adsorbed particle is equivalent to an electric dipole, it will interact with other adsorbed particles through its dipole field. The result is that the effective dipole moment of an adsorbed particle in the presence of other adsorbed particles is changed to a new value. An equation for this new value is derived in this appendix.

The model to be used is illustrated in figure 11. The α's are the po-
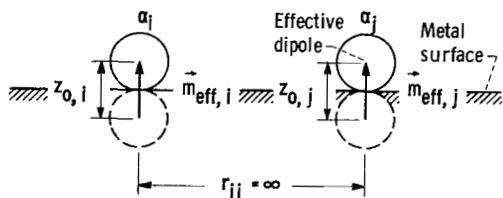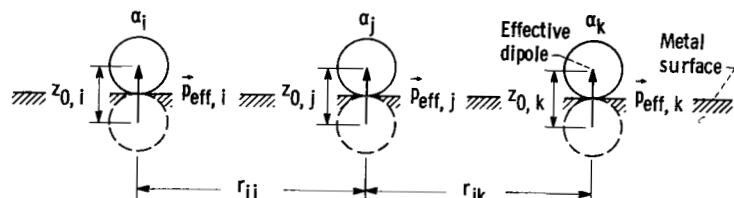
(a) Fraction of adsorption sites occupied, $\theta \to 0$.   (b) Fraction of adsorption sites occupied, $\theta > 0$.

Figure 11. – Model of adsorbed particles.

larizabilities of the adsorbed particles, the $\vec{m}_{eff}$'s and $\vec{p}_{eff}$'s are their effective dipole moments at zero coverage and at coverage θ, respectively, the z_0's are twice the distances from their centers to the metal surface, and the r's are the distances between their centers. Note also that the center of each dipole lies on the metal surface and that its direction is perpendicular to this surface.
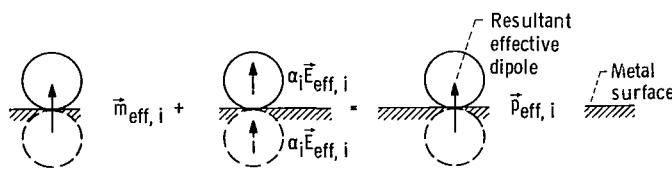
Figure 12. - Model illustrating change in effective dipole moment of adsorbed particles in presence of other adsorbed particles.

Let $\vec{E}_{eff,i}$ be the effective dipole field acting on the ith adsorbed particle. Because of this field the effective dipole moment $\vec{m}_{eff,i}$ of this particle is changed by $2\alpha_i\vec{E}_{eff,i}$ to yield a new effective dipole moment $\vec{p}_{eff,i}$ given by the relation (see fig. 12))

$$\vec{p}_{eff,i} = \vec{m}_{eff,i} + 2\alpha_i\vec{E}_{eff,i} \tag{D1}$$

The effective dipole field $\vec{E}_{eff,i}$ consists of the field $\vec{E}_{ii}$ produced by the image of the dipole $\alpha_i\vec{E}_{eff,i}$ induced in the ith adsorbed particle by $\vec{E}_{eff,i}$ and the field $\sum_{\substack{k=1 \\ k\neq i}}^{\infty} \vec{E}_{ik}$ produced by all the other effective dipoles (adsorbed particles); that is,

$$\vec{E}_{eff,i} = \vec{E}_{ii} + \sum_{\substack{k=1 \\ k\neq i}}^{\infty} \vec{E}_{ik} \tag{D2}$$

The assumption (examined in appendix H) that the field $\vec{E}_{ik}$ acting on the ith adsorbed particle is uniform and equal to $\vec{E}_{ik}$ at the surface yields

$$\vec{E}_{ii} = 2\,\frac{\alpha_i\vec{E}_{eff,i}}{z_{0,i}^3} \tag{D3}$$

and

$$\vec{E}_{ik} = -\frac{\vec{p}_{eff,k}}{r_{ik}^3} \tag{D4}$$

Substituting equations (D3) and (D4) into equation (D2) leads to the important new result

$$\vec{E}_{eff,i} = - \frac{1}{1 - \dfrac{2\alpha_i}{z_{0,i}^3}} \sum_{\substack{k=1 \\ k \neq i}}^{\infty} \frac{\vec{p}_{eff,k}}{r_{ik}^3} \tag{D5}$$

Using the previous expression for $\vec{E}_{eff,i}$ in equation (D1) yields the following equation for $\vec{p}_{eff,i}$:

$$\vec{p}_{eff,i} = \vec{m}_{eff,i} - \frac{2\alpha_i}{1 - \dfrac{2\alpha_i}{z_{0,i}^3}} \sum_{\substack{k=1 \\ k \neq i}}^{\infty} \frac{\vec{p}_{eff,k}}{r_{ik}^3}, \quad i = 1, 2, \cdots \tag{D6}$$

In matrix notation equation (D6) becomes

$$\underline{p}_{eff} = \underline{m}_{eff} - \underline{\alpha}_{eff} \, \underline{T} \, \underline{p}_{eff}$$

or

$$(\underline{U} + \underline{\alpha}_{eff} \, \underline{T})\underline{p}_{eff} = \underline{m}_{eff} \tag{D7}$$

where $\underline{U}$ is a unit matrix and $\underline{\alpha}_{eff}$, $\underline{T}$, $\underline{p}_{eff}$, and $\underline{m}_{eff}$ are defined as follows:

$$\underline{\alpha}_{eff} = \begin{bmatrix} \dfrac{2\alpha_1}{1 - \dfrac{2\alpha_1}{z_{0,1}^3}} & 0 & 0 & . & . & 0 \\ 0 & \dfrac{2\alpha_2}{1 - \dfrac{2\alpha_2}{z_{0,2}^3}} & . & . & . & 0 \\ . & . & . & . & . & . \\ 0 & 0 & . & . & . & \dfrac{2\alpha_\infty}{1 - \dfrac{2\alpha_\infty}{z_{0,\infty}^3}} \end{bmatrix} \tag{D8}$$

30

$$\underline{T} = \begin{bmatrix} 0 & \dfrac{1}{r_{12}^3} & \dfrac{1}{r_{13}^3} & \cdot & \cdot & \dfrac{1}{r_{1\infty}^3} \\[2mm] \dfrac{1}{r_{21}^3} & 0 & \dfrac{1}{r_{23}^3} & \cdot & \cdot & \dfrac{1}{r_{2\infty}^3} \\[2mm] \cdot & \cdot & \cdot & \cdot & \cdot & \cdot \\[2mm] \dfrac{1}{r_{\infty 1}^3} & \dfrac{1}{r_{\infty 2}^3} & \cdot & \cdot & \cdot & 0 \end{bmatrix} \qquad (D9)$$

$$\underline{p}_{eff} = \begin{bmatrix} \vec{p}_{eff,1} \\ \vec{p}_{eff,2} \\ \cdot \\ \cdot \\ \vec{p}_{eff,\infty} \end{bmatrix} \qquad (D10)$$

$$\underline{m}_{eff} = \begin{bmatrix} \vec{m}_{eff,1} \\ \vec{m}_{eff,2} \\ \cdot \\ \cdot \\ \vec{m}_{eff,\infty} \end{bmatrix} \qquad (D11)$$

Solving for $\underline{p}_{eff}$ yields

$$\underline{p}_{eff} = (\underline{U} + \underline{\alpha}_{eff}\, \underline{T})^{-1}\, \underline{m}_{eff} \qquad (D12)$$

where the right inverse matrix $(\underline{U} + \underline{\alpha}_{eff}\, \underline{T})^{-1}$ is defined by the condition

$$(\underline{U} + \underline{\alpha}_{eff}\, \underline{T})^{-1}\, (\underline{U} + \underline{\alpha}_{eff}\, \underline{T}) = \underline{U}$$

Expanding $(\underline{U} + \underline{\alpha}_{eff}\, \underline{T})^{-1}$ in a series yields (within the limit of convergence of the series)

$$\underline{p}_{eff} = \left[\underline{U} - \underline{\alpha}_{eff}\, \underline{T} + (\underline{\alpha}_{eff}\, \underline{T})^2 - (\underline{\alpha}_{eff}\, \underline{T})^3 + \cdots \right] \underline{m}_{eff} \qquad (D13)$$

31

The ith component of $\underline{p}_{eff}$ is then given by the equation

$$\vec{P}_{eff,i} = m_{eff,i} + \left[-\sum_{\substack{k=1 \\ k \neq j}}^{\infty} \alpha_{eff,i} \frac{1}{r_{ik}^3} + \sum_{\substack{k=1 \\ k \neq j}}^{\infty} \sum_{\substack{j=1 \\ j \neq i}}^{\infty} \alpha_{eff,i} \frac{1}{r_{ij}^3} \alpha_{eff,j} \frac{1}{r_{jk}^3} \right.$$

$$\left. -\sum_{\substack{k=1 \\ k \neq j}}^{\infty} \sum_{\substack{j=1 \\ j \neq l}}^{\infty} \sum_{\substack{l=1 \\ l \neq i}}^{\infty} \alpha_{eff,i} \frac{1}{r_{il}^3} \alpha_{eff,l} \frac{1}{r_{lj}^3} \alpha_{eff,j} \frac{1}{r_{jk}^3} + \cdots \right] \vec{m}_{eff,k} \qquad (D14)$$

where $\alpha_{eff,x}$ is the effective polarizability of the xth adsorbed particle and is defined as follows:

$$\alpha_{eff,x} = \frac{2\alpha_x}{1 - \dfrac{2\alpha_x}{z_{0,x}^3}} \qquad x = i,\ j,\ k,\ l,\ \cdots \qquad (D15)$$

Equation (D14) is the desired relation for the effective dipole moment of the ith adsorbed particle in the presence of the metal surface and all the other adsorbed particles. Substituting it (after changing the subscript i to k) for $\vec{P}_{eff,k}$ in equation (D5) leads to the following result for the effective dipole field $\vec{E}_{eff,i}$:

$$\vec{E}_{eff,i} = \frac{1}{1 - \dfrac{2\alpha_i}{z_{0,i}^3}} \sum_{\substack{k=1 \\ k \neq i}}^{\infty} \frac{1}{r_{ik}^3} \left\{ \vec{m}_{eff,k} \right.$$

$$+ \left[-\sum_{\substack{m=1 \\ m \neq k}}^{\infty} \alpha_{eff,k} \frac{1}{r_{km}^3} + \sum_{\substack{m=1 \\ m \neq j}}^{\infty} \sum_{\substack{j=1 \\ j \neq k}}^{\infty} \alpha_{eff,k} \frac{1}{r_{kj}^3} \alpha_{eff,l} \frac{1}{r_{jm}^3} \right.$$

$$\left. \left. -\sum_{\substack{m=1 \\ m \neq j}}^{\infty} \sum_{\substack{j=1 \\ j \neq l}}^{\infty} \sum_{\substack{l=1 \\ l \neq k}}^{\infty} \alpha_{eff,k} \frac{1}{r_{kl}^3} \alpha_{eff,l} \frac{1}{r_{lj}^3} \alpha_{eff,j} \frac{1}{r_{jm}^3} + \cdots \right] m_{eff,m} \right\} \qquad (D16)$$

In matrix notation the previous expression takes the form

$$\underline{E}_{eff} = (\underline{U} - \underline{\alpha}\ \underline{S})^{-1}\ \underline{T}(\underline{U} + \underline{\alpha}_{eff}\ \underline{T})^{-1}\ \underline{m}_{eff} \tag{D17}$$

or

$$\underline{E}_{eff} = \underline{\Lambda}\ \underline{m}_{eff} \tag{D18}$$

in which $\underline{\alpha}$, $\underline{S}$, $\underline{E}_{eff}$, and $\underline{\Lambda}$ are defined as follows:

$$\underline{\alpha} = \begin{bmatrix} \alpha_1 & 0 & 0 & . & . & 0 \\ 0 & \alpha_2 & 0 & . & . & 0 \\ . & . & . & . & . & . \\ 0 & 0 & 0 & . & . & \alpha_\infty \end{bmatrix} \tag{D19}$$

$$\underline{S} = \begin{bmatrix} \dfrac{2}{z_{0,1}^3} & 0 & 0 & . & . & 0 \\[2ex] 0 & \dfrac{2}{z_{0,2}^3} & 0 & . & . & 0 \\[2ex] . & . & . & . & . & . \\[1ex] 0 & . & . & . & . & \dfrac{2}{z_{0,\infty}^3} \end{bmatrix} \tag{D20}$$

$$\underline{E}_{eff} = \begin{bmatrix} \vec{E}_{eff,1} \\ \vec{E}_{eff,2} \\ . \\ . \\ \vec{E}_{eff,\infty} \end{bmatrix} \tag{D21}$$

$$\underline{\Lambda} = (\underline{U} - \underline{\alpha}\ \underline{S})^{-1}\ \underline{T}(\underline{U} + \underline{\alpha}_{eff}\ \underline{T})^{-1} \tag{D22}$$

A simple and useful expression can be obtained for $\vec{p}_{eff}$ by placing the following additional restriction on the model for the adsorbed particles. The configuration of the effective dipoles associated with the adsorbed particles is that of the Topping square array (ref. 5) as shown in figure 2(b) .

The length of the side b of each unit square making up the Topping square array is related to the surface density of adsorbed particles $N_s\theta$ by the relation

$$\frac{1}{b^2} = N_s\theta$$

When this restriction is incorporated into equation (D14), there results

$$\vec{p}_{eff} = \frac{\vec{m}_{eff}}{1 + \dfrac{2\alpha_0}{1 - \dfrac{2\alpha_0}{z_0^3}}\displaystyle\sum_{\substack{k=1\\k\neq i}}^{\infty}\frac{1}{r_{ik}^3}} \tag{D23}$$

Using Topping's value of $9.033/b^3$ for

$$\sum_{\substack{k=1\\k\neq i}}^{\infty}\frac{1}{r_{ik}^3}$$

and the effective polarizability expression (eq. (D15))

$$\alpha_{eff} = \frac{2\alpha_0}{1 - \dfrac{2\alpha_0}{z_0^3}} \tag{D24}$$

leads to the result

$$\vec{p}_{eff} = \frac{\vec{m}_{eff}}{1 + 9.033\,\alpha_{eff}(N_s\theta)^{3/2}} \tag{D25}$$

It should be noted that the new and unique feature in this equation is that α_{eff}, which is given by equation (D24), is not the polarizability of the adsorbed particle.

DETERMINATION OF AVERAGE DIPOLE MOMENT OF ith ADSORBED PARTICLE

IN PRESENCE OF INFINITE NUMBER OF OTHER ADSORBED PARTICLES -

DISTRIBUTION FUNCTION METHOD

Adsorbed particles have certain mobility on the surface of their adsorbent. For this reason the distribution of these particles on the surface constantly changes with time, and the effective dipole moment associated with each of these particles fluctuates around its average value. An equation is derived herein for this average value by the method of classical statistical mechanics. While this equation does not lend itself to evaluation, it nevertheless affords a degree of insight into the problem.

The model to be used for the adsorbed particles is the same as the one used in appendix D to derive the general equation (D14) for the effective dipole moment $\vec{p}_{eff,i}$, except for the following additional restrictions:

(1) The effective dipole moment at zero coverage associated with each adsorbed particle is identical; that is,

$$\vec{m}_{eff,1} = \vec{m}_{eff,2} = \cdot \cdot \cdot = \vec{m}_{eff,\infty} = \vec{m}_{eff}$$

(2) The polarizability of each adsorbed particle is identical; that is,

$$\alpha_1 = \alpha_2 = \cdot \cdot \cdot = \alpha_\infty = \alpha_0$$

(3) The distance from the center of each adsorbed particle to the surface of the adsorbent is identical; that is,

$$z_{0,1} = z_{0,2} = \cdot \cdot \cdot z_{0,\infty} = z_0$$

Imposing these three restrictions on the general equation (D14) for $\vec{p}_{eff,i}$ leads to the result

$$\vec{p}_{eff,i} = \left(1 - \alpha_{eff} \sum_{\substack{k=1 \\ k \neq i}}^{\infty} \frac{1}{r_{ik}^3} + \alpha_{eff}^2 \sum_{\substack{k=1 \\ k \neq j}}^{\infty} \sum_{\substack{j=1 \\ j \neq i}}^{\infty} \frac{1}{r_{ij}^3} \frac{1}{r_{jk}^3} \right.$$
$$\left. - \alpha_{eff}^3 \sum_{\substack{k=1 \\ k \neq j}}^{\infty} \sum_{\substack{j=1 \\ j \neq l}}^{\infty} \sum_{\substack{l=1 \\ l \neq i}}^{\infty} \frac{1}{r_{il}^3} \frac{1}{r_{lj}^3} \frac{1}{r_{jk}^3} + \cdot \cdot \cdot \right) \vec{m}_{eff} \quad (E1)$$

An expression is now to be derived for the statistical average of $\vec{p}_{eff,i}$ given by equation (E1). Since $\vec{p}_{eff,i}$ is a function of the interdipole distances only, its statistical average $\langle \vec{p}_{eff,i} \rangle$ is (ref. 35)

$$\langle \vec{p}_{eff,i} \rangle = \frac{\int \cdots \iint_{\mathscr{A}} \vec{p}_{eff,i} \exp\left(-\frac{V}{kT}\right) d\vec{r}_1 \cdots d\vec{r}_\infty}{Z_\infty} \tag{E2}$$

where $d\vec{r}_1 \cdots d\vec{r}_\infty$, V, and Z_∞ are, respectively, the coordinates, total potential energy, and configurational integral of the adsorbed particles. A general equation is derived in appendix D for $\vec{p}_{eff,i}$, and Z_∞ is given by

$$Z_\infty = \int \cdots \int_{\mathscr{A}} \exp\left(-\frac{V}{kT}\right) d\vec{r}_1 \cdots d\vec{r}_\infty \tag{E3}$$

Equation (E2) can also be written in the form

$$\langle \vec{p}_{eff,i} \rangle = \vec{m}_{eff} \left[1 - \frac{\alpha_{eff}}{(N_s \theta)^2 \mathscr{A}^2} \iint_{\mathscr{A}} \frac{1}{r_{ik}^3} \rho^{(2)}(\vec{r}_i, \vec{r}_k) d\vec{r}_i\, d\vec{r}_k \right.$$

$$\left. + \frac{\alpha_{eff}^2}{(N_s \theta)^3 \mathscr{A}^3} \iiint_{\mathscr{A}} \frac{1}{r_{ij}^3}\frac{1}{r_{jk}^3} \rho^{(3)}(\vec{r}_i, \vec{r}_j, \vec{r}_k) d\vec{r}_i\, d\vec{r}_j\, d\vec{r}_k - \cdots \right] \tag{E4}$$

where $\rho^{(n)}(\vec{r}_1, \cdots, \vec{r}_n)$ is the distribution function. It is defined in references 36 and 37 as follows:

$$\rho^{(n)}(\vec{r}_1, \cdots, \vec{r}_n) = \int \cdots \int_{\mathscr{A}} \rho^{(n)}(\vec{r}_1, \cdots, \vec{r}_n) d\vec{r}_1 \cdots d\vec{r}_n$$

$$\times \frac{\int \cdots \int_{\mathscr{A}} \exp\left(-\frac{V}{kT}\right) d\vec{r}_{n+1} \cdots d\vec{r}_\infty}{Z_\infty} \tag{E5}$$

The quantity $\rho^{(n)}(\vec{r}_1, \cdots, \vec{r}_n) d\vec{r}_1 \cdots d\vec{r}_n$ has the physical significance that it is the probability of finding any one of the adsorbed particles located in the volume element $d\vec{r}_1$ with center at $\vec{r}_1$, any other in $d\vec{r}_2$ with center at $\vec{r}_2$, and so forth, irrespective of the location of the other adsorbed particles.

The appropriate expression to be used for $\rho^{(2)}(\vec{r}_1, \vec{r}_2)$ in equation (E5) has recently been derived by Hill and Saitô (ref. 37). In terms of the symbols

used in this report, the relation for $\rho^{(2)}(\vec{r}_1,\vec{r}_2)$ is

$$\rho^{(2)}(\vec{r}_i,\vec{r}_k) = (N_s\theta)^2 \frac{\exp\left(-\frac{w_i}{kT}\right)\exp\left(-\frac{w_k}{kT}\right)\exp\left(-\frac{v_{ik}}{kT}\right)}{\left(\frac{Z_1}{\mathscr{A}}\right)^2}$$

$$\times \left(1 - \left(\frac{N_s\theta\mathscr{A}}{Z_1^2}\right)\left\{2\iint_{\mathscr{A}}\exp\left(-\frac{w_i}{kT}\right)\exp\left(-\frac{w_k}{kT}\right)\left[\exp\left(-\frac{v_{ik}}{kT}\right) - 1\right]d\vec{r}_i\,d\vec{r}_k\right.\right.$$

$$\left.\left. - Z_1\int_{\mathscr{A}}\exp\left(-\frac{w_j}{kT}\right)\left[\exp\left(-\frac{v_{ij}}{kT}\right)\exp\left(-\frac{v_{jk}}{kT}\right) - 1\right]d\vec{r}_j\right\} + \cdots \right) \qquad (E6)$$

where Z_1 represents the configurational integral for one particle, or,

$$Z_1 = \iint_{\mathscr{A}}\exp\left(-\frac{w}{kT}\right)d\vec{r} \qquad (E7)$$

It can be shown that $\rho^{(3)}(\vec{r}_i,\vec{r}_j,\vec{r}_k)$ is

$$\rho^{(3)}(\vec{r}_i,\vec{r}_j,\vec{r}_k)$$

$$= (N_s\theta)^3 \frac{\exp\left(-\frac{w_i}{kT}\right)\exp\left(-\frac{w_j}{kT}\right)\exp\left(-\frac{w_k}{kT}\right)\exp\left(-\frac{v_{ij} + v_{ik} + v_{jk}}{kT}\right)}{\left(\frac{Z_1}{\mathscr{A}}\right)^3}(1 - \cdots) \qquad (E8)$$

Combining equations (E5), (E6), and (E8) yields

$$\langle\vec{p}_{eff,i}\rangle = \vec{m}_{eff}\left[1 - \frac{\alpha_{eff}}{Z_1^2}\iint_{\mathscr{A}}\frac{1}{r_{ik}^3}\exp\left(-\frac{w_i + w_k + v_{ik}}{kT}\right)\left(1 - \frac{N_s\theta\mathscr{A}}{Z_1^2}\left\{2\iint_{\mathscr{A}}\exp\left(-\frac{w_{i'} + w_{k'}}{kT}\right)\right.\right.\right.$$

$$\times\left.\left.\left[\exp\left(-\frac{v_{i'k'}}{kT}\right) - 1\right]d\vec{r}_{i'}\,d\vec{r}_{k'} - Z_1\int_{\mathscr{A}}\exp\left(-\frac{w_j}{kT}\right)\left[\exp\left(-\frac{v_{ij} + v_{jk}}{kT}\right) - 1\right]d\vec{r}_j\right\} + \cdots\right)d\vec{r}_i\,d\vec{r}_k \qquad (E9)$$

$$\left. + \frac{\alpha_{eff}^2}{Z_1^3}\iiint_{\mathscr{A}}\frac{1}{r_{ij}^3}\frac{1}{r_{jk}^3}\exp\left(-\frac{w_i + w_j + w_k + v_{ij} + v_{ik} + v_{jk}}{kT}\right)(1 - \cdots)d\vec{r}_i\,d\vec{r}_j\,d\vec{r}_k\right]$$

Only the first two terms of $\rho^{(2)}(\vec{r}_i, \vec{r}_k)$ and the first term of $\rho^{(3)}(\vec{r}_i, \vec{r}_j, \vec{r}_k)$ are written out in equation (E9). This means that the average operation specified by this equation gives the correct average value of $\vec{p}_{eff,i}$ only if the ith adsorbed particle does not interact with more than two of its neighbors at any one time. At surface coverage greater than about one-third, additional terms from $\rho^{(2)}$, $\rho^{(3)}$, $\rho^{(4)}$, and so forth must be included.

Equation (E9) as it stands is extremely difficult to evaluate numerically, but it does show clearly how the various interaction energy terms enter into the determination of the average value of the effective dipole moment $\vec{p}_{eff,i}$.

APPENDIX F

GENERAL EQUATION FOR MUTUAL ELECTROSTATIC POTENTIAL ENERGY

OF GAS PARTICLES ADSORBED ON METAL SURFACE

As indicated in appendix D, atoms adsorbed on a metal surface are polarized, or both ionized and polarized by the surface. In either case the adsorbed particle and its image constitute to first order an electric dipole. As a result, a system of adsorbed particles will have a mutual electrostatic potential energy V_{el} in addition to its interaction energy W with the surface. Thus, the total energy V of the system is given by

$$V = W + V_{el} \tag{F1}$$

In this appendix a general equation is derived for V_{el}. The model and symbols used are identical to those in appendix D (see figs. 11 and 12, pp. 28 and 29). The energy V_{el} may be split into the internal energy V_{in} and the external energy V_{ex}; that is,

$$V_{el} = V_{in} + V_{ex} \tag{F2}$$

The internal energy V_{in} is the polarization energy, which is given by the equation

$$
\begin{aligned}
V_{in} &= \sum_{i=1}^{\infty} \int_{\vec{m}_{eff,i}/2}^{\vec{p}_{eff,i}/2} \vec{E}_{eff,i} \cdot d\,\frac{\vec{p}_{eff,i}}{2} \\[2mm]
&= \sum_{i=1}^{\infty} \alpha_i \int_{0}^{\vec{E}_{eff,i}} \vec{E}_{eff,i} \cdot d\vec{E}_{eff,i} \\[2mm]
&= \frac{1}{2} \sum_{i=1}^{\infty} \alpha_i \vec{E}_{eff,i} \cdot \vec{E}_{eff,i}
\end{aligned} \tag{F3}
$$

The external energy is the effective dipole field interaction energy of the adsorbed particles, which is given by the equation

$$V_{ex} = -\sum_{i=1}^{\infty} \frac{\vec{p}_{eff,i}}{2} \cdot \vec{E}_{eff,i} \tag{F4}$$

Combining equations (F2), (F3), and (F4) yields

$$V_{e\ell} = \frac{1}{2} \sum_{i=1} \left(\alpha_i \vec{E}_{eff,i} \cdot \vec{E}_{eff,i} - \vec{p}_{eff} \cdot \vec{E}_{eff,i} \right) \tag{F5}$$

In matrix notation equation (F5) takes the form

$$V_{e\ell} = \frac{1}{2} \left(\underline{E}_{eff}^t \, \underline{\alpha}^t \, \underline{E}_{eff} - \underline{p}_{eff}^t \, \underline{E}_{eff} \right) \tag{F6}$$

Substituting equations (D18) and (D12) of appendix D into the previous expression for E_{eff} and p_{eff}, respectively, leads to the result

$$V_{e\ell} = \frac{1}{2} \left\{ (\underline{\Lambda} \, \underline{m}_{eff})^t \, \underline{\alpha}^t + \left[(\underline{U} + \underline{\alpha}_{eff} \, \underline{T})^{-1} \, \underline{m}_{eff} \right]^t \right\} \underline{\Lambda} \, \underline{m}_{eff} \tag{F7}$$

which is the desired result.

VARIATION IN ATOM DESORPTION ENERGY WITH COVERAGE

When an atom is adsorbed on a metal surface, it stays on the surface for an average time τ before desorbing as an atom or as an ion. In general, the mean adsorption time τ of the adsorbed particle may be expressed in the form $\tau = [\tau_0/f(\theta)]\exp[(\varphi_0 + \Delta\varphi)/kT_s]$, where τ_0 is a constant, φ_0 is its desorption energy when there are no other particles adsorbed on the surface, and $\Delta\varphi$ is the change in its desorption energy when it is surrounded by other adsorbed particles. In this appendix, an equation is derived for the change $\Delta\varphi_a$ in the desorption energy φ_a of an adsorbed particle desorbing as an atom.

The two models shown, respectively, in figure 10 (see p. 28) in appendix D are used for the adsorbed particles. In the first model the adsorbed particles are represented by polarized adatoms (adsorbed atoms), while in the second model they are represented by polarized adions (adsorbed ions). The common features of these two models are as follows (see fig. 2, p. 3 also):

(1) There is an infinite number (but finite surface density) of adsorbed particles on the surface.

(2) All adsorbed particles are alike; that is, they are either all polarized adatoms or all polarized adions.

(3) The polarizability α_0 of each adsorbed particle and its effective dipole moments $\vec{m}_{eff}$ and $\vec{p}_{eff}$ at zero coverage and at coverage θ, respectively, are the same as any other adsorbed particles on the surface.

(4) The center of each effective dipole lies on the surface plane of the metal, and its direction is perpendicular to this plane.

(5) The dipoles have the Topping square array configuration. The distance between adjacent dipoles b is related to the surface density $N_s\theta$ of adsorbed particles at all coverages by $1/b^2 = N_s\theta$.

The method to be used for determining $\Delta\varphi_a$ is identical to the one used in appendix F to derive the mutual electrostatic potential energy for the adsorbed particles. Applying this method to the case where the adsorbed particles are represented by polarized adatoms leads to the following expression for $\Delta\varphi_a$:

$$\Delta\varphi_a = -\left(\frac{1}{2}\,\alpha_0|\vec{E}_{eff}|^2 - \frac{\vec{p}_{eff}}{2}\cdot\vec{E}_{eff}\right) \tag{G1}$$

The first term within the parenthesis in equation (G1) is the polarization energy, and the second term is the interaction energy of the adsorbed particles and the effective dipole field acting on them, where $\vec{E}_{eff}$ is the effective dipole field introduced by equation (D1) in appendix D.

For the case in which the adsorbed particles are represented by polarized adions,

$$\Delta\varphi_a = -\left(\frac{1}{2}\,\alpha_0|\vec{E}_{eff}|^2 - \frac{\vec{p}_{eff} - \vec{m}_1}{2}\cdot\vec{E}_{eff} + \varphi_{i,E_{eff}}\right) \tag{G2}$$

Since the surface plane of the metal is an equipotential plane, $\varphi_{i,E_{eff}}$ can be determined as follows:

$$\varphi_{i,E_{eff}} = -\int_0^{z_0/2} Ze\vec{E}_{eff}\cdot\hat{n}\,dz$$

$$= -\vec{E}_{eff}\cdot\hat{n}Ze\,\frac{z_0}{2}$$

$$= -\vec{E}_{eff}\cdot\frac{\vec{m}_1}{2} \tag{G3}$$

In the previous derivation $\vec{E}_{eff}$ is assumed constant over the distance $0 \leq z \leq \frac{z_0}{2}$.

Substituting equation (G3) for $(\varphi_i)_{E_{eff}}$ in equation (G2) leads to the result

$$\Delta\varphi_a = -\left(\frac{1}{2}\,\alpha_0|\vec{E}_{eff}|^2 - \frac{\vec{p}_{eff}}{2}\cdot\vec{E}_{eff}\right) \tag{G4}$$

which is identical to equation (G1). For this reason, regardless of which of the two models shown in figure 10 (see p. 28) is used for the adsorbed particles, the previous expression can be used to determine $\Delta\varphi_a$.

The next step is to express the right side of equation (G4) in terms of the parameters $|\vec{m}_{eff}|$, α_{eff}, N_s, and $z_0/2$ and the variable θ. Using the definitions for α_{eff} and $\vec{E}_{eff}$ introduced in appendix D (see eqs. (D15) and (D1)) leads to the result

$$\Delta\varphi_a = -\frac{1 + \dfrac{\alpha_{eff}}{z_0^3}}{4\alpha_{eff}}\left(|\vec{m}_{eff}|^2 - |\vec{p}_{eff}|^2\right) \tag{G5}$$

Applying equation (C5) and

$$\vec{p}_{eff} \cdot \hat{n} = \pm |\vec{p}_{eff}| \tag{G6}$$

to equation (G5) yields

$$\Delta \varphi_a = -\frac{1 + \dfrac{\alpha_{eff}}{z_0^3}}{4\alpha_{eff}} \left[|\vec{m}_{eff}|^2 - \frac{1}{4\pi^2 e^2 N_s^2} \left(\frac{\Delta \varphi_e}{\theta} \right)^2 \right] \tag{G7}$$

Equation (G7) applies to both models of adsorbed particles shown in figure 10 (see p. 28). Care must be taken in applying equation (G7), however, since the definition of $\vec{m}_{eff}$ depends on which model is used.

EXAMINATION OF VALIDITY OF IDEAL DIPOLE AND

UNIFORM FIELD ASSUMPTIONS

Throughout this report the effective dipole associated with each adsorbed particle has been treated as an ideal dipole; that is, equation (B3) instead of (B5) is used to represent the field produced by each effective dipole. In addition, it is assumed that the dipole field acting on each adsorbed particle is uniform and equal to the value at the surface. The validity of both of these assumptions is now examined.
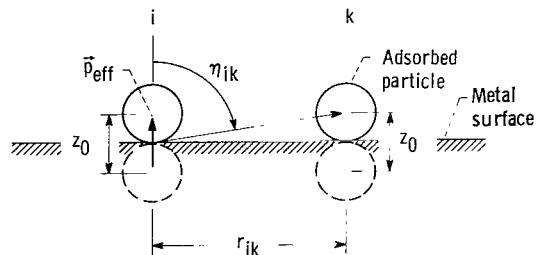
Figure 13. - Model of adsorbed particles used for checking ideal dipole and uniform field assumptions.

With the aid of equations (B3), (B6), and figure 13, it may be shown that at the metal surface the ratio of the field $(\vec{E}_{ik,nid})_{z=0}$ produced by a nonideal dipole to the field $(\vec{E}_{ik,id})_{z=0}$ produced by an ideal dipole is

$$\frac{(\vec{E}_{ik,nid})_{z=0}}{(\vec{E}_{ik,id})_{z=0}} = \left[1 + \frac{1}{4}\left(\frac{z_0}{r_{ik}}\right)^2 \right]^{-3/2} \tag{H1}$$

Also, it may be shown that the ratio of the normal component (to the surface) of the field $(\vec{E}_{ik,id})_{z=z_0/2}$ produced by an ideal dipole at the center of the adsorbed particle to the field $(\vec{E}_{ik,id})_{z=0}$ at the surface is

$$\frac{(\vec{E}_{ik,id})_{z=z_0/2}}{(\vec{E}_{ik,id})_{z=0}} = 1 - 3(\cos \eta_{ik})^2 \tag{H2}$$

Using 3.00 A for z_0 (see eq. (15)), the Topping square array for the dipole configuration, and 4.8×10^{14} per square centimeter for the maximum surface density of adsorbed particles yields

$$1 \geq \frac{\displaystyle\sum_{\substack{k=1 \\ k \neq i}}^{\infty} (\vec{E}_{ik,nid})_{z=0}}{\displaystyle\sum_{\substack{k=1 \\ k \neq i}}^{\infty} (\vec{E}_{ik,id})_{z=0}} > 0.916 \qquad \text{for} \quad 0 \leq N_s\theta \leq 4.8 \times 10^{14}/\text{sq cm} \tag{H3}$$

and

$$1 \geq \frac{\displaystyle\sum_{\substack{k=1 \\ k \neq i}}^{\infty} (\vec{E}_{ik,id})_{z=z_0/2}}{\displaystyle\sum_{\substack{k=1 \\ k \neq i}}^{\infty} (\vec{E}_{ik,id})_{z=0}} > 0.826 \qquad \text{for} \quad 0 \leq N\,\theta \leq 4.8 \times 10^{14}/\text{sq cm} \qquad \text{(H4)}$$

Since

$$\left(\frac{\displaystyle\sum_{\substack{k=1 \\ k \neq i}}^{\infty} \vec{E}_{ik,nid}}{\displaystyle\sum_{\substack{k=1 \\ k \neq i}}^{\infty} \vec{E}_{ik,id}} \right)_{z=z_0/2} \simeq \left(\frac{\displaystyle\sum_{\substack{k=1 \\ k \neq i}}^{\infty} \vec{E}_{ik,nid}}{\displaystyle\sum_{\substack{k=1 \\ k \neq i}}^{\infty} \vec{E}_{ik,id}} \right)_{z=0} \qquad \text{(H5)}$$

it follows that

$$1 \geq \frac{\displaystyle\sum_{\substack{k=1 \\ k \neq i}}^{\infty} (\vec{E}_{ik,nid})_{z=z_0/2}}{\displaystyle\sum_{\substack{k=1 \\ k \neq i}}^{\infty} (\vec{E}_{ik,id})_{z=0}} > 0.756 \qquad \text{for} \quad 0 \leq N_s\,\theta \leq 4.8 \times 10^{14}/\text{sq cm} \qquad \text{(H6)}$$

From the foregoing analysis, it may be seen that the ideal dipole and the uniform field assumptions introduce a maximum error of +24 percent into the field calculation. Because of this error, the values of α_{eff} and z_0 determined in this report are also too large by zero to +24 percent and zero to +7 percent (in the first approximation), respectively. The error is zero at zero coverage and rises to its maximum value at coverage of unity.

GRAPHS OF RICHARDSON-DUSHMAN EQUATION

Thermionic emission of a metal is generally represented by the Richardson-Dushman equation

$$J_s = A_0 T^2 \exp\left(-\frac{\varphi_e}{kT}\right) \tag{I1}$$

For the rapid determination of J_s from known values of φ_e and T, or φ_e from known values of J_s and T, a series of eight graphs of the Richardson-Dushman equation is presented in figure 14. In these graphs J_s is plotted against T with φ_e as the parameter. The range of J_s, T, and φ_e are as follows: J_s, 10^{-9} to 10^{+3} amperes per square centimeter; T, $500°$ to $3500°$ K; φ_e, 0.5 to 8.0 electron volts, which is increased in steps of $\Delta\varphi_e = 0.05$ electron volt. The values $A_0 = 120$ amperes per square centimeter per $(°K)^2$ and $k = 1/11,606$ electron volts per $°K$ were used for the calculations.
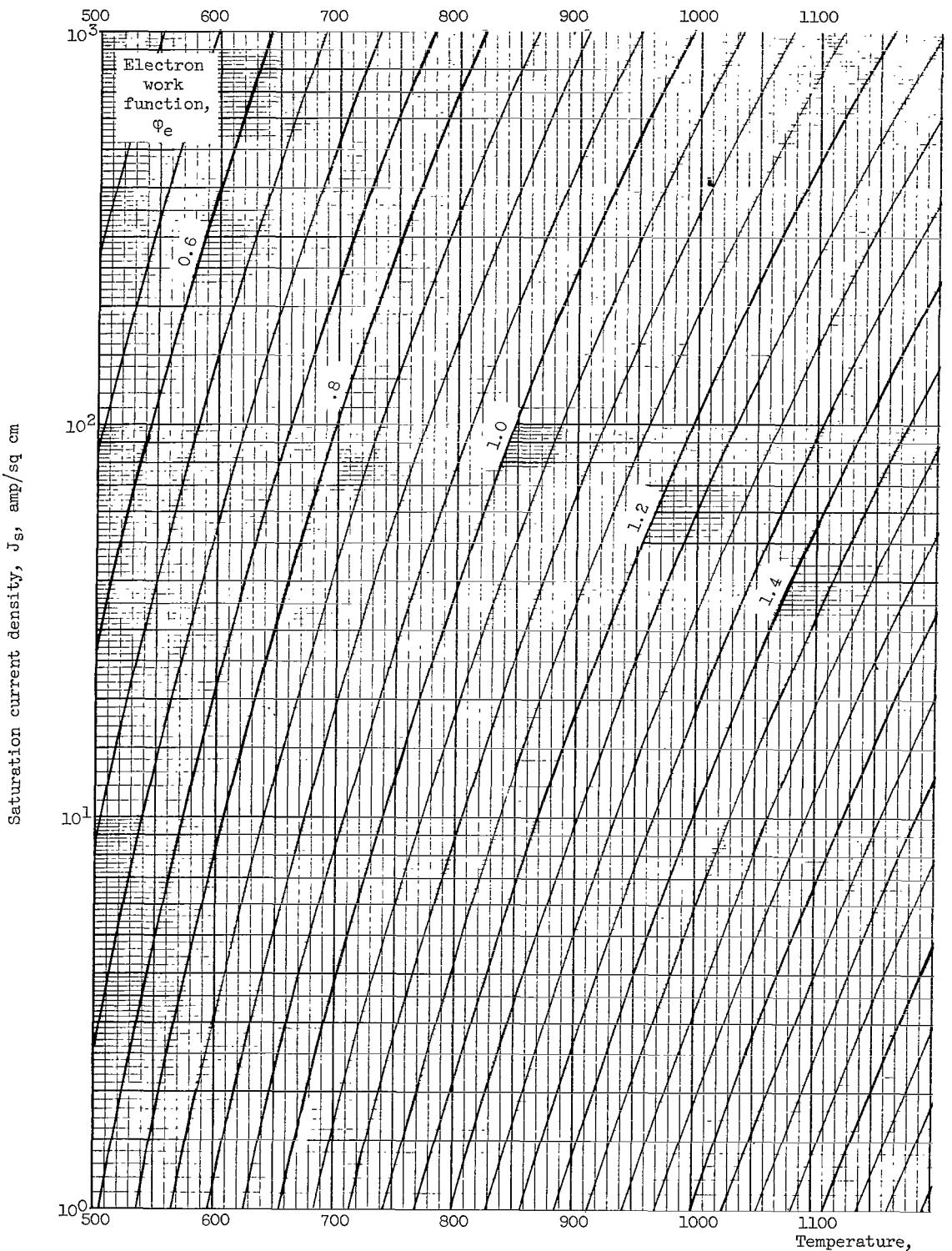
(a) Saturation current density, 10^0 to 10^3 amperes per

Figure 14. – Graphs of Richardson-

square centimeter; temperature, 500° to 2000° K.

Dushman equation (eq. (11)).
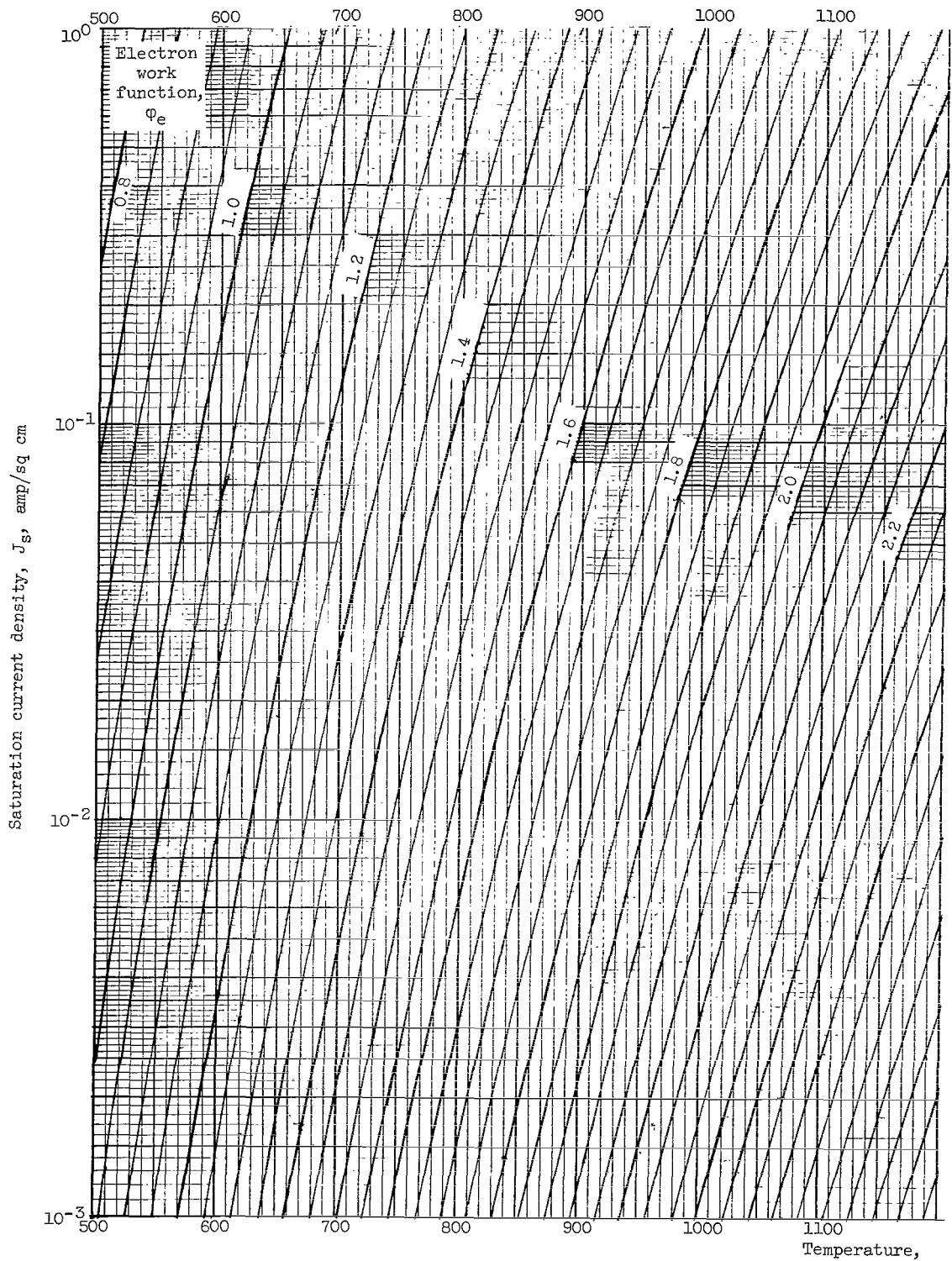
(b) Saturation current density, 10^{-3} to 10^0 amperes per

Figure 14. – Continued. Graphs of

square centimeter; temperature, 500° to 2000° K.

Richardson-Dushman equation (eq. (11)).

(c) Saturation current density, 10^{-6} to 10^{-3} ampere per

Figure 14. – Continued. Graphs of
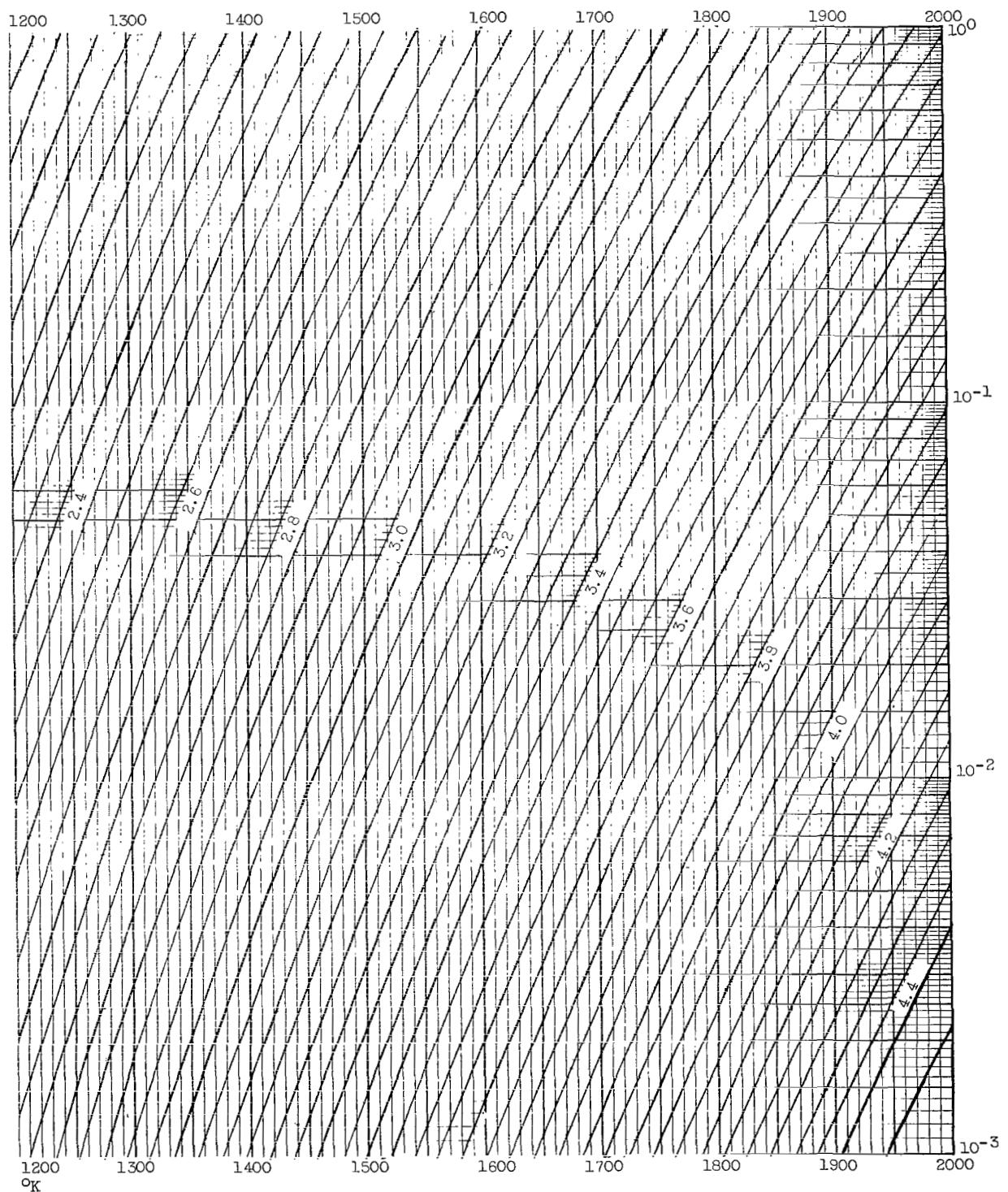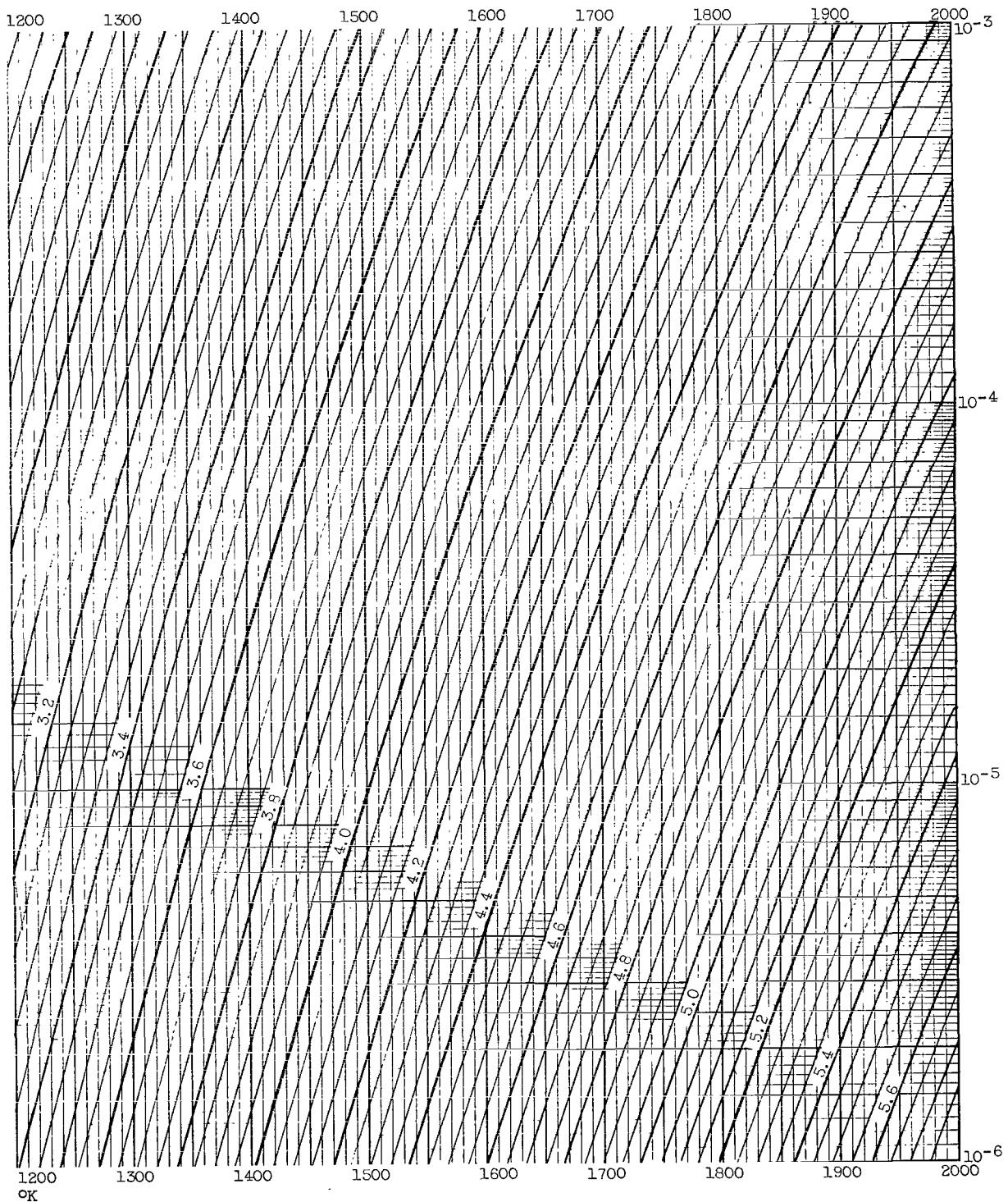
square centimeter; temperature, 500^0 to 2000^0 K.

Richardson-Dushman equation (eq. (11)).
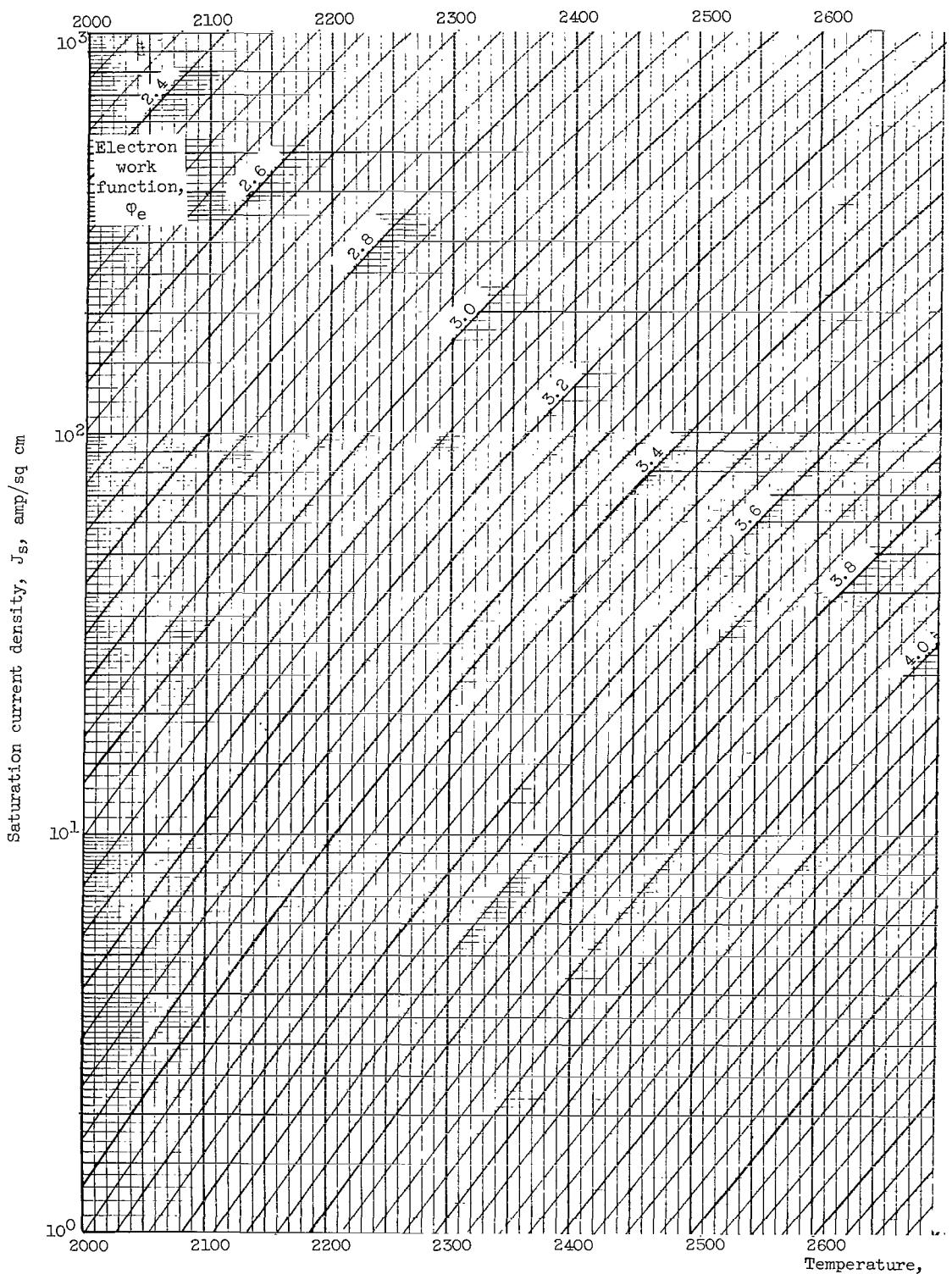
(d) Saturation current density, 10^{-9} to 10^{-6} ampere per

Figure 14. – Continued. Graphs of

54

square centimeter; temperature, 500° to 2000° K.

Richardson-Dushman equation (eq. (11)).

(e) Saturation current density, 10^0 to 10^3 amperes per

Figure 14. - Continued. Graphs of
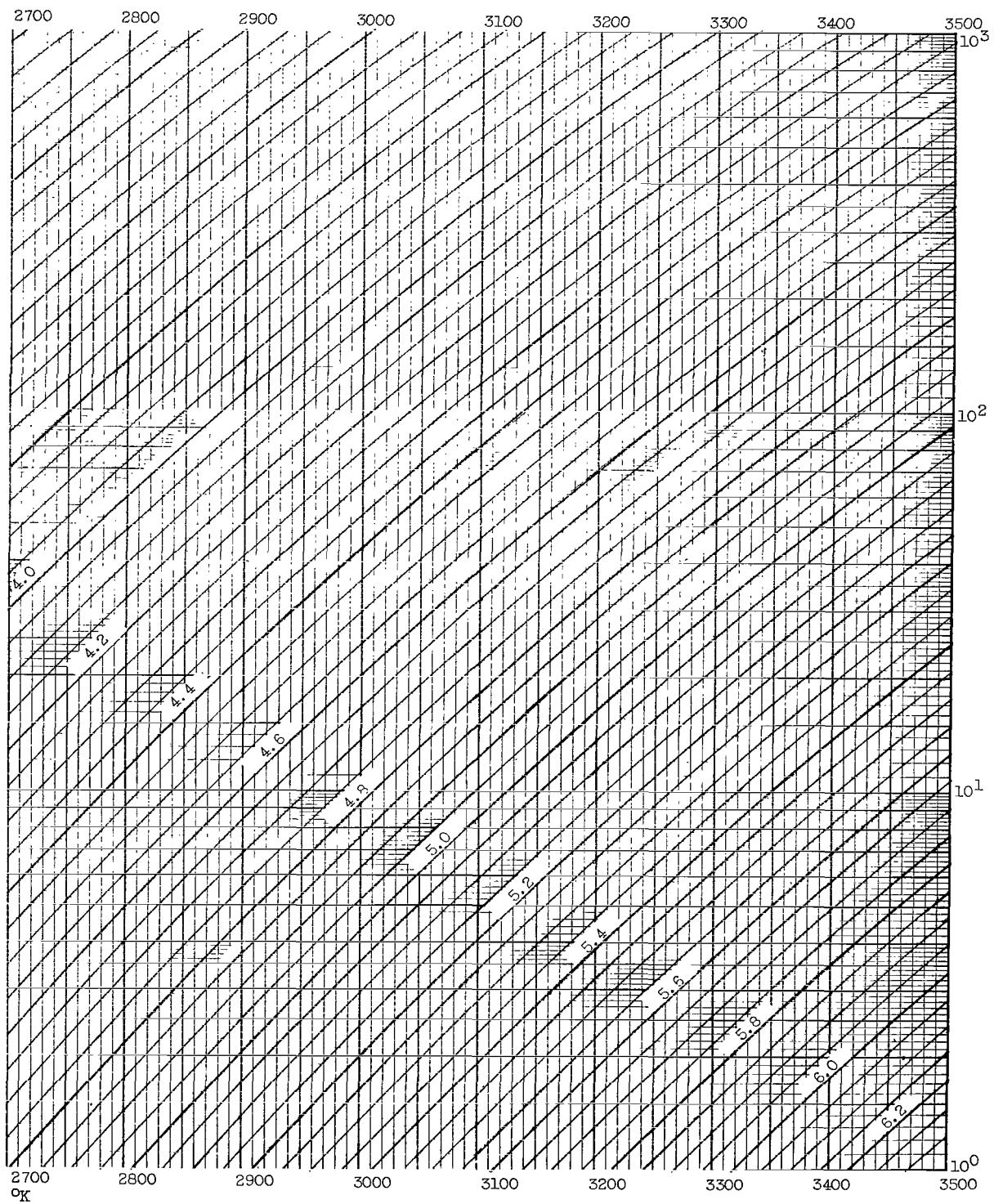
square centimeter; temperature, 2000° to 3500° K.

Richardson-Dushman equation (eq. (11)).

(f) Saturation current density, 10^{-3} to 10^0 amperes per

Figure 14. – Continued. Graphs of

square centimeter; temperature, 2000^0 to 3500^0 K.

Richardson-Dushman equation (eq. (11)).
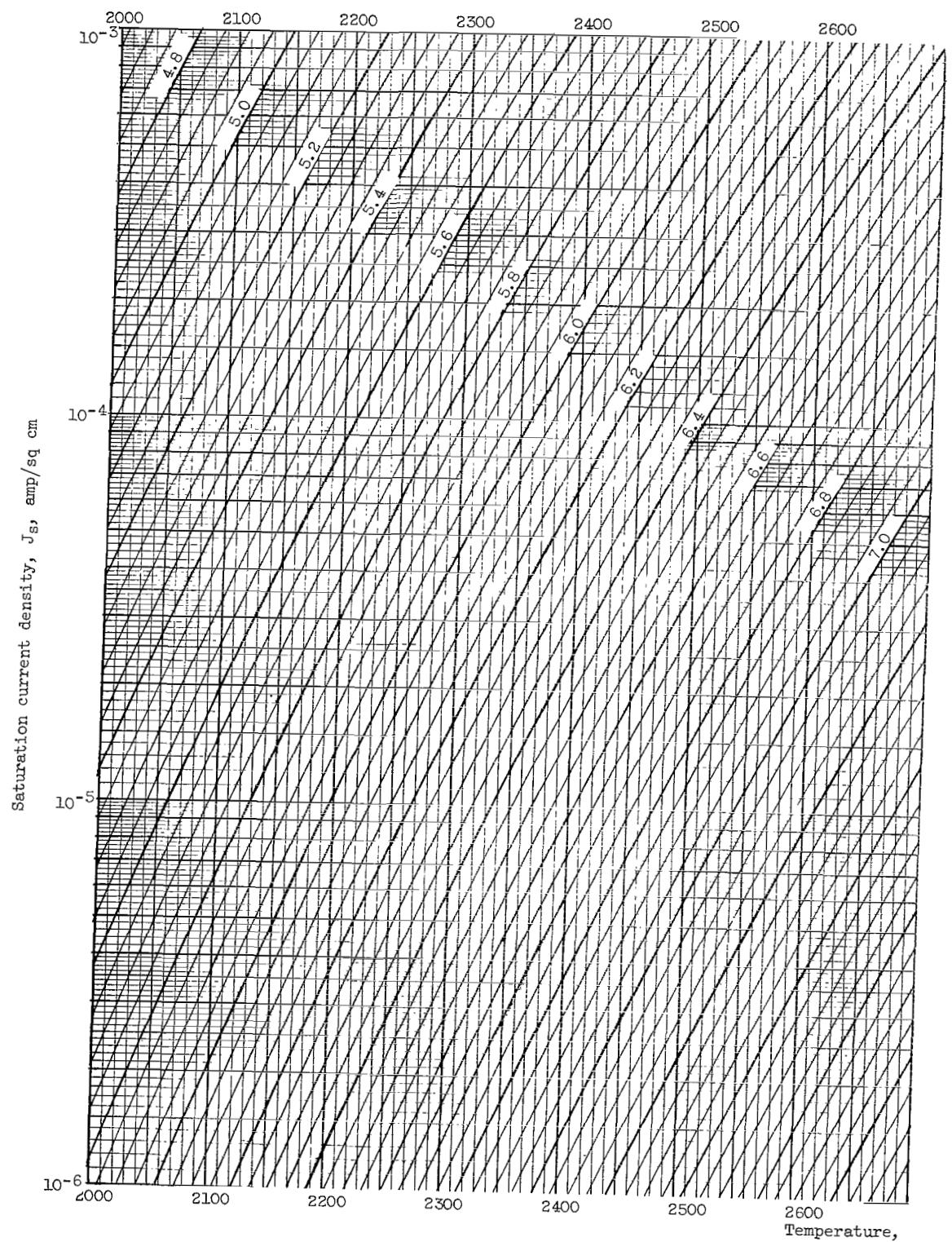
(g) Saturation current density, 10^{-6} to 10^{-3} ampere per

Figure 14. - Continued. Graphs of
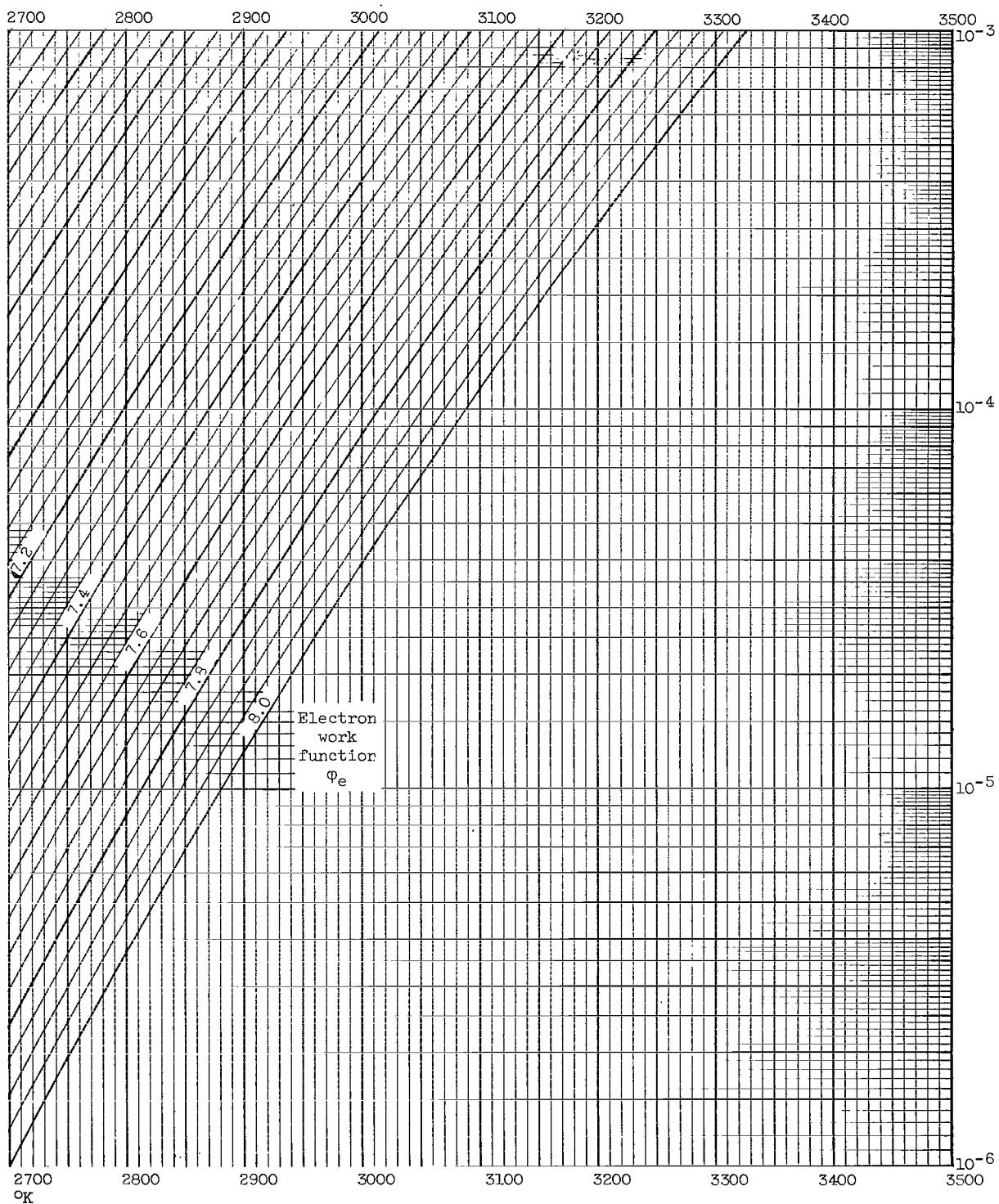
square centimeter; temperature, 2000^0 to 3500^0 K.

Richardson-Dushman equation (eq. (11)).
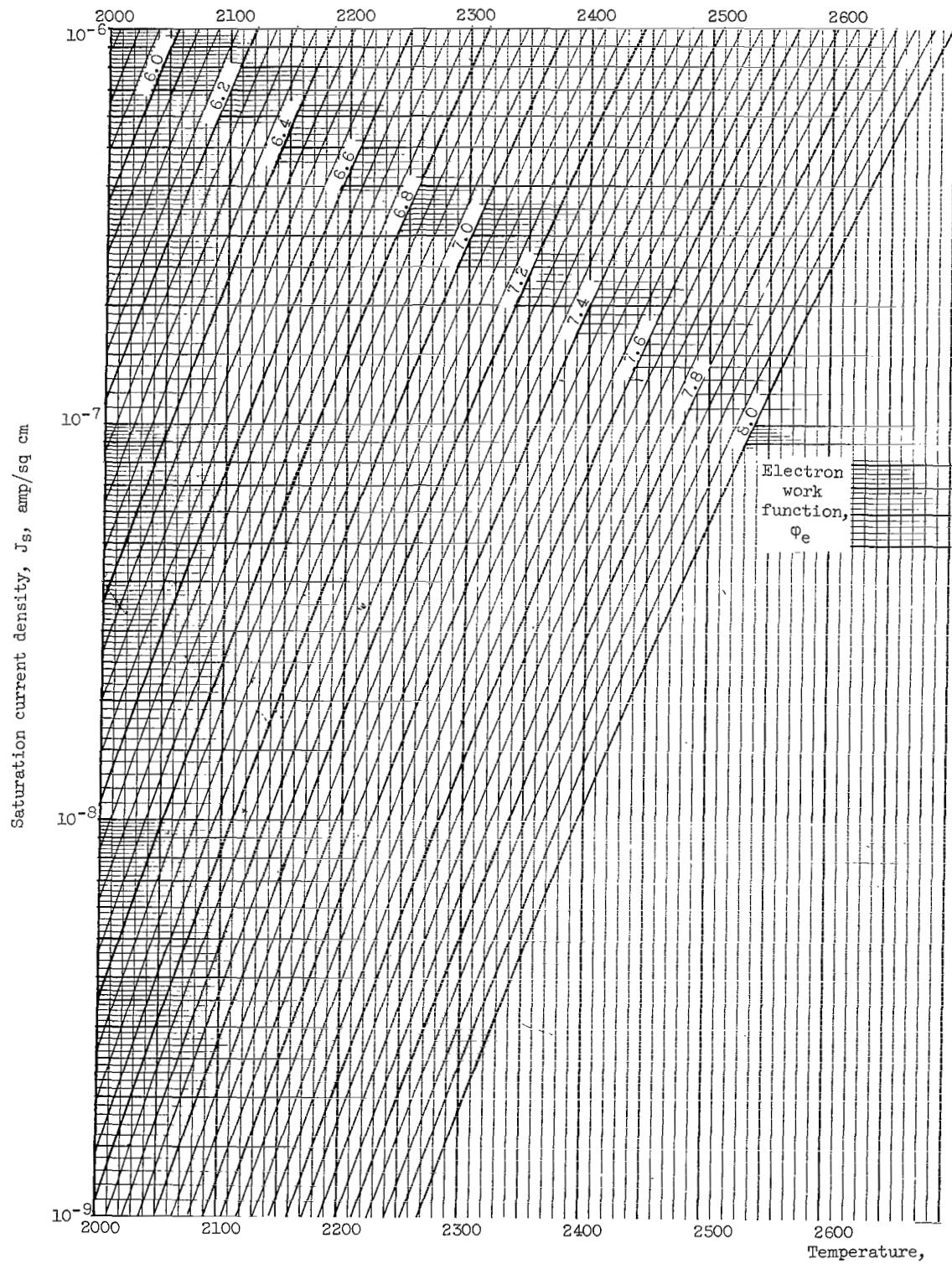
(h) Saturation current density, 10^{-9} to 10^{-6} ampere per

Figure 14. – Concluded. Graphs of
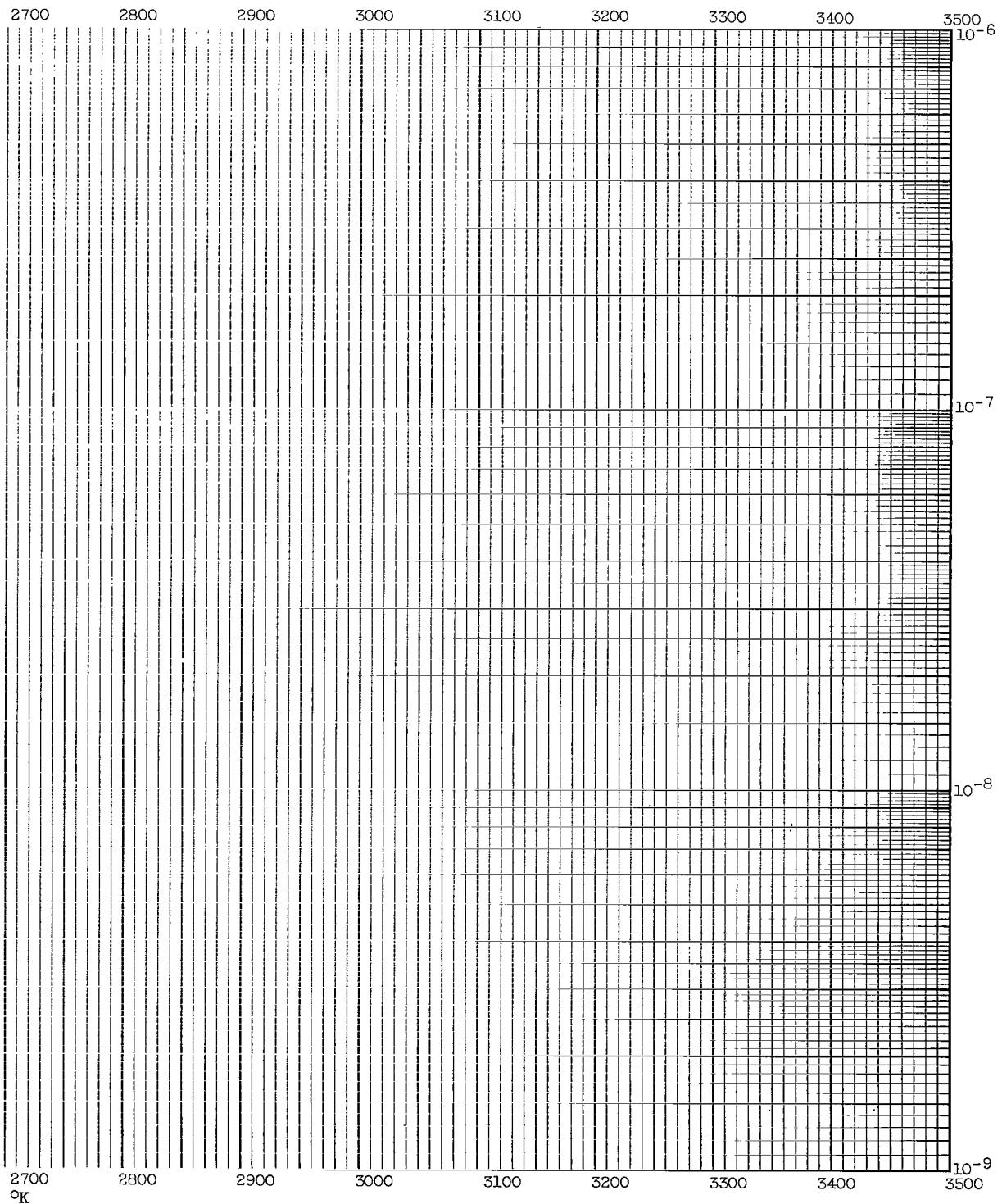
square centimeter; temperature, 2000⁰ to 3500⁰ K.

Richardson-Dushman equation (eq. (11)).

REFERENCES

1. Houston, John M.: Thermionic Emission of Refractory Metals in Cesium
     Vapor. Power Information Center-Proceedings of the Round Table Discus-
     sion on Cathode Emission Investigations and Experimental Techniques for
     Fabrication and Operating Thermionic Cells. Univ. of Pa., PIC-ELE-TI
     3/3, June 1961.

2. Mignolet, J. C. P.: Theoretical and Experimental Study of Some Problems of
     Adsorption. Mem. Soc. Roy. Sci. Liege, ser. 5, vol. 1, no. 3, 1958, pp.
     7-162. (In French.)

3. Culver, R. V., and Tompkins, F. C.: Surface Potentials and Adsorption
     Process on Metals. Vol. 11 of Advances in Catalysis, Academic Press,
     Inc., 1959, pp. 67-131.

4. Eberhagen, A.: Die Änderung der Austrittsorbeit von Metallen durch eine
     Gasadsorption. (The Alteration of Work Function of Metals by Adsorption
     of Gas) Fortachr. Physik, bd. 8, nos. 5-6, 1960, pp. 245-294.

5. Topping, J.: On the Mutual Potential Energy of a Plane Networks of Dou-
     blets. Proc. Roy. Soc. (London), ser. A, vol. 114, Feb. 1, 1927, pp.
     67-72.

6. deBoer, J. H.: Adsorption Phenomena. Vol. 8 of Advances in Catalysis,
     Academic Press, Inc., 1956, pp. 17-161.

7. Ehrlich, Gert, and Hudda, F. G.: Interaction of Rare Gases with Metal Sur-
     faces. I. A, Kr, and Xe on Tungsten. Jour. Chem. Phys., vol. 30,
     no. 2, Feb. 1959, pp. 493-511.

8. Zingerman, Ya. P., Ishchuk, V. A., and Morozovakii, V. A.: Adsorption of
     Atoms of the Alkali Earth Group by Polycrystalline Tungsten. Soviet
     Phys. - Solid State, vol. 3, no. 4, Oct. 1961, pp. 760-766.

9. Gyftopoulos, Elias P., and Levine, Jules D.: Work Function Variation of
     Metals Coated by Metallic Films. Jour. Appl. Phys., vol. 33, no. 1, Jan.
     1962, pp. 67-73.

10. Copley, M. J., and Phipps, T. E.: The Surface Ionization of Potassium on
     Tungsten. Phys. Rev., vol. 48, Dec. 15, 1935, pp. 960-968.

11. Langmuir, I.: Vapor Pressures, Evaporation, Condensation and Adsorption.
     Jour. Am. Chem. Soc., vol. 54, 1932, pp. 2798-2832.

12. Taylor, John Bradshaw, and Langmuir, Irving: The Evaporation of Atoms,
     Ions, and Electrons from Cesium Films on Tungsten. Phys. Rev., vol. 44,
     no. 6, Sept. 15, 1933, pp. 423-458.

13. Scheer, Milton D., and Fine, Joseph: Kinetics of Cs^+ Desorption from
     Tungsten. Jour. Chem. Phys., vol. 37, no. 1, July 1962, pp. 107-113.

14. Herzberg, Gerhard: Atomic Spectra and Atomic Structure. Second ed., Dover Publications, 1944, p. 201.

15. Hughes, F. L.: Mean Adsorption Lifetime of Rb on Etched Tungsten Single Crystals: Neutrals. Phys. Rev., vol. 113, no. 4, Feb. 15, 1959, pp. 1036-1038.

16. Hughes, F. L., and Levinstein, H.: Mean Adsorption Lifetime of Rb on Etched Tungsten Single Crystals: Ions. Phys. Rev., vol. 113, no. 4, Feb. 15, 1959, pp. 1029-1036.

17. Scheer, Milton D., and Fine, Joseph: Kinetics of Desorption. II. Cs^+ and Ba^+ from Rhenium. Jour. of Chem. Phys., vol. 38, no. 2, Jan. 15, 1963, pp. 307-309.

18. deBoer, J. H.: The Dynamical Character of Adsorption. Oxford University Press, 1953, pp. 30-36.

19. Taylor, John B., and Langmuir, Irving: Vapor Pressure of Cesium by the Positive Ion Method. Phys. Rev., vol. 51, May 1, 1937, pp. 753-760.

20. Breitwieser, Roland: Cesium Diode Operation in Three Modes. Report on 23rd Annual Conf. on Physical Electronics, M.I.T., March 20-22, 1963, p. 267.

21. Fajans, K., and Joos, G.: Mass Refraction of Ions and Molecules in the Light of the Atom Structure. Z. Physik, vol. 23, 1924, pp. 1-46.

22. Born, M., and Heisenberg, W.: The Effect of the Deformability of Ions on the Optical and Chemical Constants. Z. Physik, vol. 23, 1924, pp. 388-410.

23. Pauling, L.: Theoretical Prediction of the Physical Properties of Many-Electron Atoms and Ions. Mole Refraction, Diamagnetic Susceptibility, and Extension in Space. Proc. Roy. Soc. (London), vol. A114, 1927, pp. 181-211.

24. Tessman, Jack R., Kahn, A. H., and Shockley, William: Electronic Polarizabilities of Ions in Crystals. Phys. Rev., vol. 92, no. 4, Nov. 15, 1953, pp. 890-895.

25. Sternheimer, R. M.: Electronic Polarizabilities of Ions. Phys. Rev., vol. 115, no. 5, Sept. 1, 1959, pp. 1198-1206.

26. Salop, Arthur, Pollack, Edward, and Bederson, Benjamin: Measurements of the Electric Polarizabilities of the Alkalis Using the E-H Gradient Balance Method. Phys. Rev., vol. 124, no. 5, Dec. 1, 1961, pp. 1431-1438.

27. Chamberlain, George E., and Zorn, Jens C.: Alkali Polarizabilities by the Atomic Beam Electrostatic Deflection Method. Phys. Rev., vol. 129, no. 2, Jan. 15, 1963, pp. 677-680.

28. Sternheimer, R. M.: Electronic Polarizabilities of the Alkali Atoms. Phys. Rev., vol. 127, no. 4, Aug. 15, 1962, pp. 1220-1223.

29. Goldschmidt, V. M.: Geochemische Verteilungsgesetze der Element. (Geochemical Distribution Laws of the Elements.) Shrifter Norske Videnskaps-Akad. Oslo, I. Mat.-Naturv. Kl. Vol. 1926. No. 8, 1927, pp. 7-156.

30. Pauling, Linus: The Nature of Chemical Bond and the Structure of Molecules and Crystals. Third ed., Cornell Univ. Press, 1960.

31. Gourary, B. S., and Adrain, F. J.: Wave Functions for Electron-Excess Color Centers in Alkali Halide Crystals. Vol. 10 of Solid State Physics. F. Seitz, and D. Turnbull, ed., Academic Press, 1960, pp. 143-146.

32. Barrett, Charles S.: Structure of Metals, Crystallographic Methods, Principles, and Data. Second ed., McGraw-Hill Book Co., Inc., 1952, pp. 646-648.

33. Becker, J. A.: Adsorption on Metal Surfaces and Its Bearing on Catalysis. Vol. 7 of Advances in Catalysis, Academic Press, Inc., 1955, pp. 135-211.

34. Gavrikyuk, V. M.: Adsorptsiya atomin bariyn i molekul okisu bariyn na vol'frami. (Adsorption of Barium Atoms and Barium Oxide Molecules on Tungsten.) II. Ukrayin fiz. Zh. (USSR), vol. 4, no. 6, 1959, pp. 734-749.

35. ter Haar, D.: Elements of Statistical Mechanics. Holt, Rinehart and Winston, 1960, ch. 2.

36. Hill, T. L.: Statistical Mechanics: Principles and Selected Applications. McGraw-Hill Book Co., Inc., 1956, ch. 6.

37. Hill, Terrell L., and Saitô, Nohuhiko: Statistical Mechanics of Monatomic Systems in an External Periodic Potential Field. II. Distribution Function Theory for Fluids. Jour. Chem. Phys., vol. 34, no. 5, May 1961, pp. 1543-1553.

NASA SCIENTIFIC AND TECHNICAL PUBLICATIONS

TECHNICAL REPORTS: Scientific and technical information considered important, complete, and a lasting contribution to existing knowledge.

TECHNICAL NOTES: Information less broad in scope but nevertheless of importance as a contribution to existing knowledge.

TECHNICAL MEMORANDUMS: Information receiving limited distribution because of preliminary data, security classification, or other reasons.

CONTRACTOR REPORTS: Technical information generated in connection with a NASA contract or grant and released under NASA auspices.

TECHNICAL TRANSLATIONS: Information published in a foreign language considered to merit NASA distribution in English.

TECHNICAL REPRINTS: Information derived from NASA activities and initially published in the form of journal articles.

SPECIAL PUBLICATIONS: Information derived from or of value to NASA activities but not necessarily reporting the results of individual NASA-programmed scientific efforts. Publications include conference proceedings, monographs, data compilations, handbooks, sourcebooks, and special bibliographies.

Details on the availability of these publications may be obtained from:

SCIENTIFIC AND TECHNICAL INFORMATION DIVISION

NATIONAL AERONAUTICS AND SPACE ADMINISTRATION

Washington, D.C. 20546